PRINTED/ADDITIVELY MANUFACTURED AND COMPACT ANTENNAS FOR IOT AND WEARABLE APPLICATIONS

A Thesis
Presented to
The Academic Faculty

by

Kunal A. Nate

In Partial Fulfillment
of the Requirements for the Degree
Master of Science in the
School of Electrical and Computer Engineering

Georgia Institute of Technology
May 2016

PRINTED/ADDITIVELY MANUFACTURED AND COMPACT ANTENNAS FOR IOT AND WEARABLE APPLICATIONS

Approved by:

Dr. Manos M. Tentzeris, Advisor
School of Electrical and Computer Engineering
Georgia Institute of Technology

Dr. Andrew Peterson
School of Electrical and Computer Engineering
Georgia Institute of Technology

Dr. Waymond Scott
School of Electrical and Computer Engineering
Georgia Institute of Technology

Date Approved: 04 / 29 / 2016

To my father, mother, brother

ACKNOWLEDGEMENTS

I would like to express the deepest appreciation to my advisor, Dr. Manos Tentzeris, who has the attitude and the substance of a genius: he continually and convincingly conveyed a spirit of adventure in regard to research. Without his guidance and support this dissertation would not have been possible.

I would like to thank my committee members, Dr. Andrew Peterson and Dr. Waymond Scott, for being excellent professor and providing me with insightful feedback on this work.

I am highly indebted and thoroughly grateful to Jimmy Hester for his persistent support and untiring teaching. My sincerest gratitude goes out to my fellow ATHENA lab mates, Nauroze, Daniel, Christy, Jo, John, Bijan, Ryan, Su for their constant guidance and their support in completing this endeavor. I would like to express my special gratitude and thanks to Michael Isakov for providing me novel materials to study.

Finally and most importantly, I would like to thank my roommates, friends and family for bringing best out of me. None of this would have been possible without their unending love and support.

TABLE OF CONTENTS

LIST OF TABLES

LIST OF FIGURES

Page

SUMMARY

The research provided in this thesis focuses on the development of the novel additively manufactured antennas using the additive 3-D and material inkjet printing fabrication as well as the conventional subtractive manufacturing by using milling machine for the compact Internet of Things (IoT) and wearable applications. The initial part of the work focuses on the different ways of fabrication of the additively manufactured antenna that includes Finite Deposition Method (FDM) and PolyJet 3-D printing technique for the substrate material fabrication. And the material inkjet printing for the conductive radiating antenna element fabrication. The document discusses the unconventional issue of the surface roughness in the 3-D printed substrates materials. The later part focuses on the designing and testing techniques for the compact electrically small antennas (ESA) for the compact IoT applications.

Chapter 1 introduces the need for the additive manufacturing (AM) in the packaging industry.

Chapter 2 outlines the modern additive manufacturing techniques that include FDM and PolyJet 3-D printing for substrate fabrication and the material inkjet printing technique for the conductive traces printing.

Chapter 3 describes the utilization of the printing techniques discussed to fabricate the antennas.

The work presented in Section 3.1 was published in 2014 European Microwave Week (EuMW) Proceedings.

The work presented in Section 3.2 was published in 2014 IEEE Electrical Performance of Electronic Packaging (EPEPS) Proceedings.

Chapter 4 presents the design, fabrication, and measurement of electrically small planar rectangular spiral antenna operating at 433 MHz. This also explains the design and fabrication of the Wheeler cap to measure the radiation efficiency of the antenna.

CHAPTER I

INTRODUCTION

Printing technologies have been playing an ever increasing role as fabrication methods over the last decade. Additive manufacturing (AM) processes can reduce waste, cut the cost of tooling and materials, speed up production, and enable designs that might not be feasible with conventional production processes. The AM technology has already been used on the factory floor to manufacture complex plastic and even metal parts [1-2]. Additive manufacturing uses a combination of new technologies to manufacture objects by depositing many consecutive thin layers of material. This flexibility allows fabrication of complex components and significantly shortens their fabrication process, from numerical model to final product. However, such technique has not been demonstrated up till now for the fabrication of the multilayer RF components at GHz frequencies. A combination of 3-D printing, a very effective method for thick dielectric deposition, and inkjet printing for the fabrication method capable of depositing metal layers for the fabrication of components that could work efficiently even at the radio frequencies could offer an entirely new methodology for antenna and RF circuit fabrication. This thesis demonstrates this technology through the examples of the antennas fabricated with additive manufacturing technique.

1.1 Need of AM in semiconductor industry:

Because of certain inherent advantages over traditional subtractive manufacturing, this fabrication topology has the potential to make a huge impact on the semiconductor industry. The following paragraph explains the need and the anticipation of the potential impact of additive manufacturing in the semiconductor industry:

For more than four decades, the semiconductor industry has rigorously followed Moore's law in scaling down a transistor size through fabrication techniques. Moore's law states that the number of transistors per square inch on integrated circuits would be doubled

every year. This trend has been followed since the integrated circuits were invented. Gordon Moore, co-founder of Intel predicted that this tendency would continue for the foreseeable future. Semiconductor Industry has been widely using a horizontal or 2-D System-On- Chip (SoC) approach which is a system integration approach that integrates a number of transistors as well as mixed-signal active and passive components together. As the semiconductor industry seems to be on the verge of saturation towards horizontal miniaturization of the integrated systems [3]. There has been focus shifted towards 3-D stacked System-in-Package (SiP) to make systems compact as well as cost effective by shortening the wire interconnects. However, SiP systems are still limited by manufacturing processes just as SoC systems [4]. Designers can take SiP a step further by embedding both active and passive components, but passive component embedding is bulky and requires thick film. Thick-film component embedding distinguishes SiP from System-on-Package (SoP), a 3-D solution that incorporates vertical stacking of the packages, embedding the active and passive components. This makes systems more compact and more cost effective than ever [3].

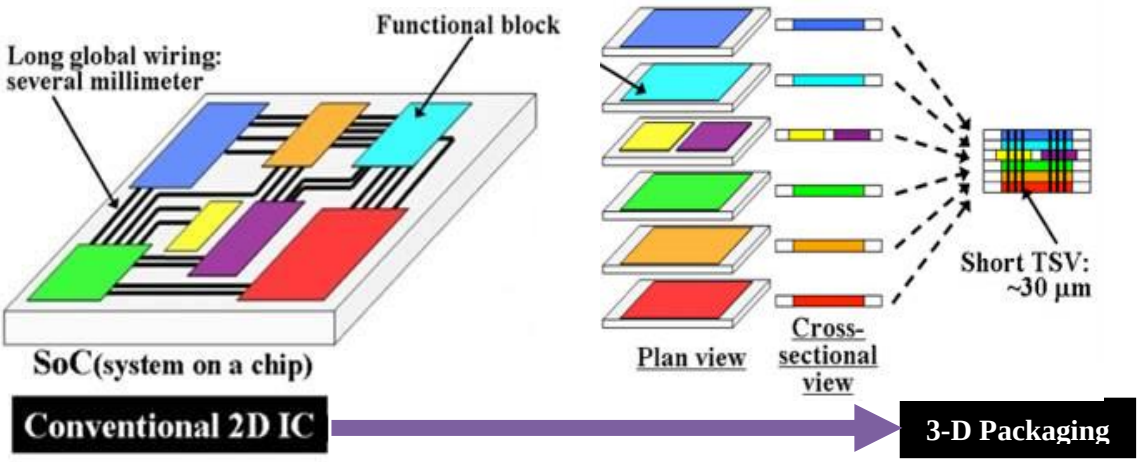

Figure 1.1 Comparison of 2-D IC packaging to 3-D packaging [5]

Electronic products continue to find new applications in personal, wearable, portable, healthcare, entertainment, automotive, environmental and security systems as well as IoTs. Industry demands compact, light-weight and low cost packaging solutions. The

vision was to integrate 3-D stacked packages of digital, analog, sensors, RF, optical systems together with 3-D printed packaging.

1.2 Issues with a current solution:

3-D system packaging with the Through Silicon Vias (TSV) interconnects is one of the emerging options today and considered as a new paradigm for the semiconductor industry. Although some small level of production has been reported, the adoption rate in the high volume manufacturing (HVM) is still very small due to unresolved challenges. Most of the conference speakers agreed that the thin wafers often used for TSV fabrication pose significant handling issues, such as bubbles that can develop on the adhesive used to bond the active wafer to the silicon or the glass. This causes the thin wafer to easily bow with cracks developing at the wafer's edge. Another problem is the Coefficient of Thermal Expansion (CTE) mismatches, causing materials to separate under temperature changes. Despite the fact that in the 3-D SiP noise coupling between the various mixed signals modules can be minimized by the decoupling capacitors, it limits inter-layer access in 3-D stacking. Many speakers in the conferences on TSVs noted that the fabrication cost must not exceed $150 per wafer, a target that represents a steep challenge for the industry. It is also estimated that more than 50% of the time and the resources are consumed by the verification of designs [7]. Hence to overcome all these problems and fulfil the need of the semiconductor industry it is necessary to search for other 3-D packaging solutions.

1.3 Five breakthrough advantages over traditional ways of fabrication:

1. This rapid-prototyping manufacturing process has the ability to realize same day prototypes which reduces prototyping time. Lead time, and there after design verification can be greatly reduced with the ability to test new designs rapidly. In a world where "cost

(of design) is the greatest threat to the continuation of the semiconductor roadmap," 3D printing has been shown to reduce lead times by as much as 94%.

2. Low end-product cost due to the availability of cheap 3-D printable material for packaging and also the 3-D stacked compact design reduces the length of the interconnects [6]. Due to the additive manufacturing technique, it leaves less or no waste material compared to the conventional subtractive manufacturing such as photolithography.

3. 3-D printing technology allows designers to create complicated structures with the higher degrees of freedom than the conventional methods. The process offers unit-level customization with the local manufacturing [6]. This makes the packaging useful in wearable applications as it has already proven its importance in the low cost 3-D printed prosthetics [7].

4. Low initial installation cost of manufacturing equipment assembly compared to traditional IC manufacturing processes. In the near future, enhanced 3-D printing may eventually be employed to manufacture the end-use electronic packages [8]. Experts suggest 2017 will be the breakthrough year for 3D printing since the industry's big players like HP and GE have shifted their focus on building the 3-D printers for high speed and high quality mass production [7].

5. Rapid increase in the availability of different 3-D printable materials, with each exhibiting unique properties makes a rich material library for designer and manufacturer to fabricate electronic products for numerous applications. Recently developed 3-D printable carbon fiber and nylon combination can achieve the strength to weight ratio greater than 6061 aluminium, commonly used in the fabrication of aircraft structures such as wings and fuselages [8]. Such materials would be useful in the high strength and extreme condition electronic packaging applications. The combination of nylon and carbon fiber exert EM shielding properties [8] useful in the mixed-signal multilayer applications. Bio Range materials developed by ASIGA are safe for long-term contact

with skin, making it useful for health monitoring and wearable electronic applications [9]. Flexible materials such as NinjaFlex can be useful in applications such as human motion detection [11], the tactile sensing for the artificial or “smart” skin and the flexible electronics applications [14]. Ceramics can be printed as well, leading to low loss, high temperature and power systems.

However, there are fundamental issues with plastic packaging which are still subject to research and cannot be ignored. The following are the issues that were observed in [10], [11]. 1) Plastics are prone to the moisture penetration and it affects long term reliability of the packaging. 2) Surface roughness could be a dominant issue at the higher frequencies. 3) Most of the 3-D printed materials show lossy characteristics at the RF frequencies. The plastic packaging durability and the reliability tests will be performed referring to experiments done in [12]. Many of these issues can be resolved with the use of 3D printed ceramics, offering low temperature co-fired ceramic level performance of power handling, losses, and temperature operability.

CHAPTER II

ADDITIVE MANUFACTURING TECHNIQUES

2.1 3-D Printing technique

2.1.1 Fused Deposition Modelling:

Among several different methods of 3-D printing, the Fused Deposition Modeling (FDM) technology is the most widely used technique [17]. Typical FDM 3-D printers use a thermoplastic filament as a cartridge material in the form of plastic threads or filaments which are unwounded from a coil and fed to the extrusion head. The material is heated to its melting point at the extrusion head and then extruded out of the extrusion nozzle, layer by layer, to create a three dimensional object. The Hyrel printer based on FDM technique was utilized to fabricate the substrate material. Hyrel has 50 μm 3 axes positional accuracy and 1 μm z-axis resolution or minimum possible printable layer height.

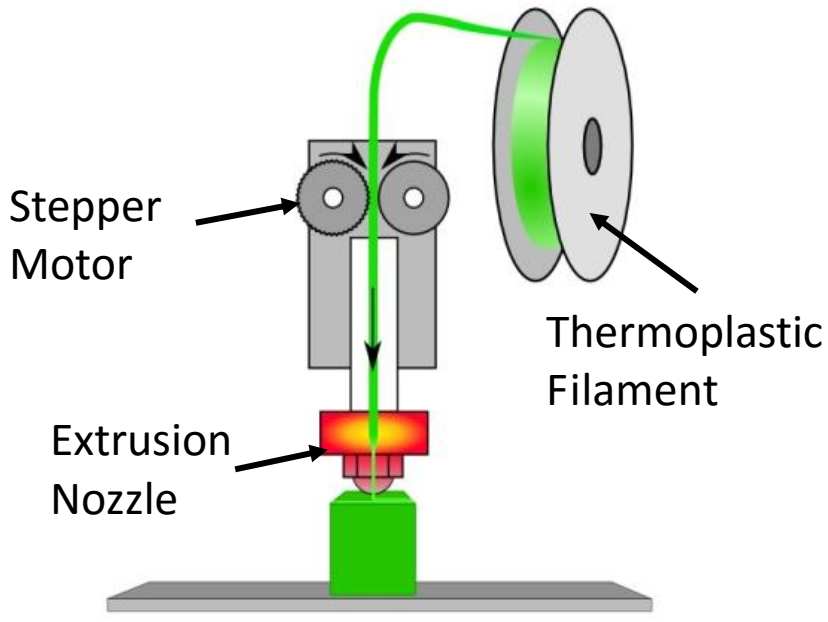

Figure 2.1 Fused Deposition Modeling based 3-D Printer [18]

Interchangeable print heads give numerous material printing capability including clay, Plasticine, Sugru, Silicon RTV, porcelain, ABS, PLA, NinjaFlex etc. The flexible NinjaFlex material was employed in Hyrel 3-D printer to fabricate flexible substrate for the antenna and the RF strain sensor.

2.1.2 PolyJet 3-D Printing:

An Objet Connex 260 3-D printer was utilized in the prototyping the antenna structure. It employs PolyJet 3-D printing technology. It has the accuracy of 15 microns which provides high precision. It is similar to inkjet document printing, but instead of jetting drops of ink onto paper, PolyJet 3-D Printers jets layers of liquid photopolymer on the build tray and cure them with UV light.

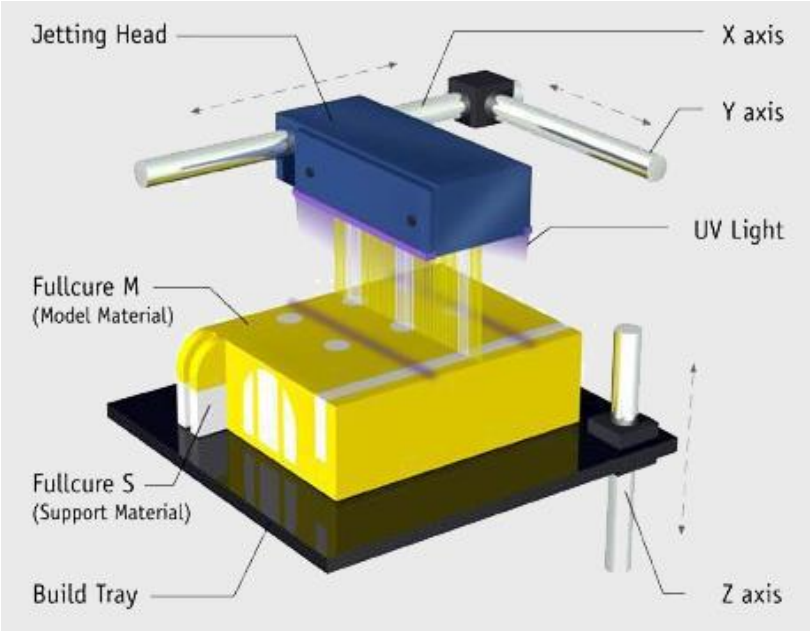

Figure 2.2 PolyJet 3-D Printing technique [19]

The PolyJet 3-D printing follows 3 steps in the fabrication process:

I. Pre-processing: Once the CAD file is uploaded in the build-preparation software, it automatically calculates the placement of the photopolymers and the support material required in the particular places for the uploaded CAD file.

II. Production: The 3-D printer jets the tiny droplets of the liquid photopolymer on the build platform and instantly solidifies with the UV curing. Fine layers accumulate on the build platform to create one or multiple 3-D models at a time. For the complex structures or overhangs 3-D printer jets the removable support material in the required locations.

III. Support removal: After removing the 3-D printed prototype out of the 3-D printer the support material can be removed by hand, with water or by using the solution bath technique.

2.2 Material Inkjet Printing:

Inkjet printing is a type additive manufacturing technique gaining its popularity from the past decade. The Dimatix Material Inkjet Printer was utilized to fabricate the conductive traces of the antenna prototype. It has the ability to print a wide range of materials including dielectrics and conductive inks with the very high resolution that can support the fabrication of the sub-terahertz passive components.

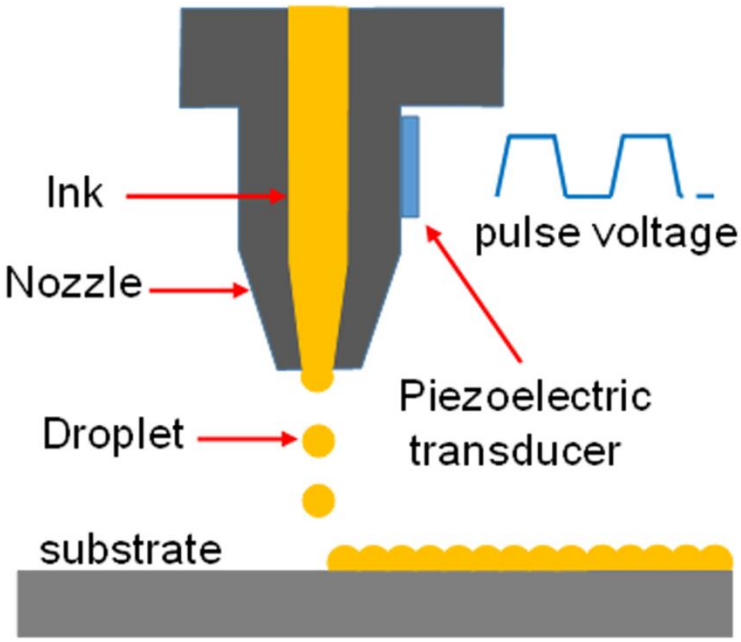

Figure 2.3 Material inkjet printing technique [20]

Material inkjet printing works in the “drop on demand” (DOD) manner similar to the office inkjet printers. First, the bitmap structure file should be uploaded in the software which is acting as an interface with the material inkjet printer. After setting the droplet size and the angle of printing the tiny inkjet nozzles are loaded with the small drops of the material to be deposited. These nozzles then jet the droplets of the material towards the substrate material placed on the build platform. The build platform and/or the nozzles are moved with the motorized system to deposit droplets on the necessary positions to form the desired pattern. Upon hitting the substrate material, the drop solvent which is carrying the material to be deposited either gets absorbed in the substrate or evaporates leaving the patterned material.

2.3 3-D Printed Substrate Metallization:

The material inkjet printing has been utilized to realize the electronic and RF components. However, most of the work is in the research domain. Almost all the published work related to the material inkjet printing was performed on the smooth substrate materials. Hence, surface roughness issue for the rough substrate materials was not discussed in detail before. The 3-D printed substrate materials can be very rough depending on multiple factors such as the type of the 3-D printing, type of the material used, minimum possible layer height and printing precision.

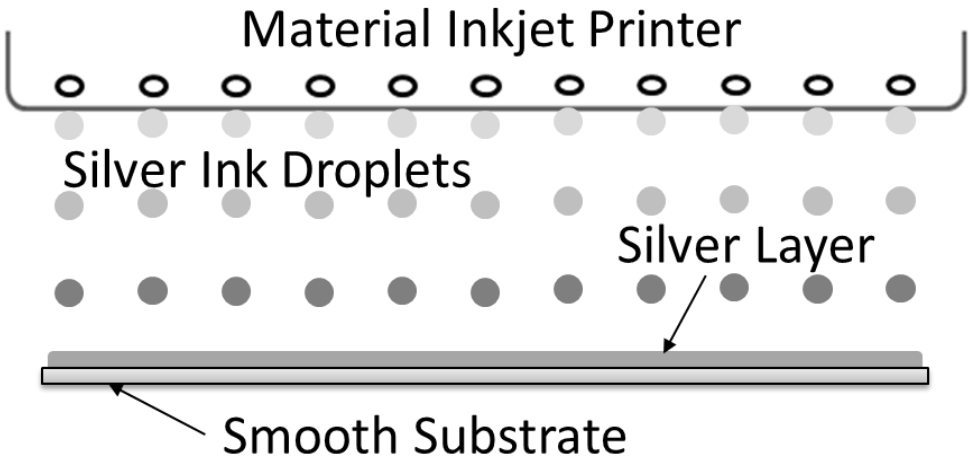

Figure 2.4 Material inkjet printing on smooth substrate

Figure 2.4 illustrates the metallization of the smooth substrate by using material inkjet printer similar to the trending RF components fabrication on the Kapton polyamide film substrates and papers.

As we discussed one of the surface roughness differentiating parameter is the technique of 3-D printing. Here we utilized 3-D printing based on PolyJet printing and Fused Deposition Modelling (FDM) technique. The substrate material printed with the PolyJet 3-D printing technique was chosen for the fully printed antenna structure because of its ability to produce smoother dielectric substrates than most of the other 3-D printing techniques.

The 3-D printed substrate materials were scanned under profilometer to measure the surface roughness. Figure 2.5 shows the surface roughness of Verowhite, an acrylic-based photopolymer material used as a substrate material for the fully printed antenna. Objet Connex PolyJet 3-D printer was utilized to fabricate the substrate material.

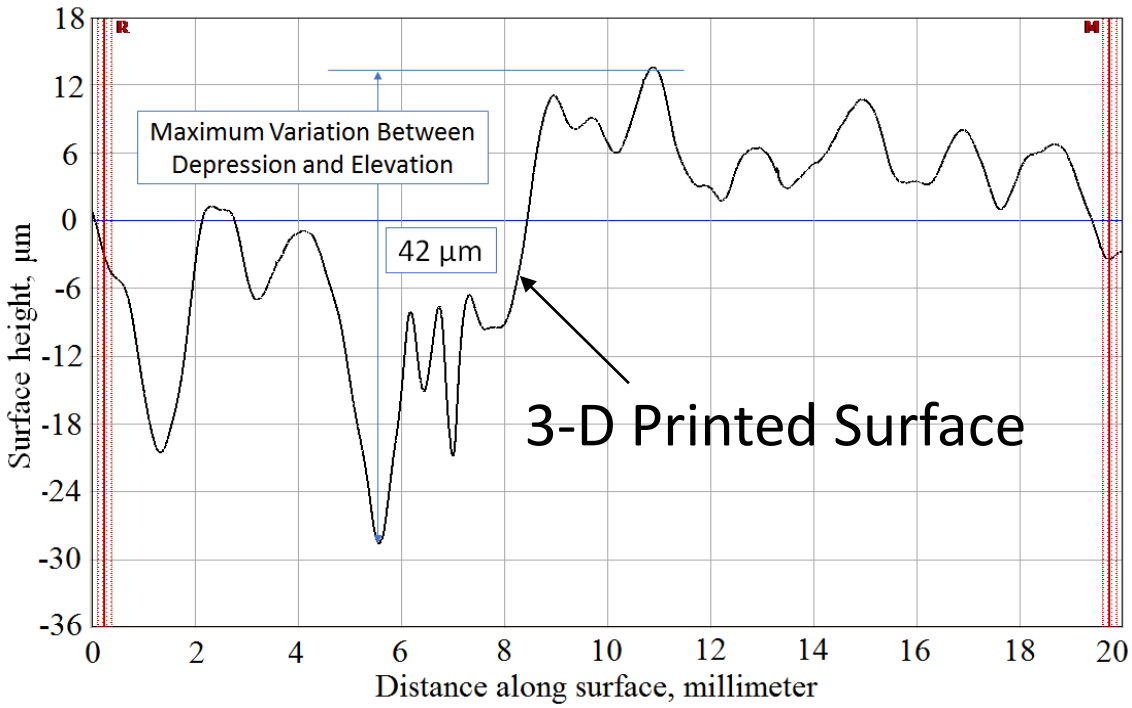

Figure 2.5 Surface roughness measurement of PolyJet 3-D printed Verowhite substrate material using Profilometer

The results show that the random variation in the surface roughness magnitude with the variation magnitude difference between the highest elevation and the deepest depression traced was 42 μm. Hence, the metallization of such surfaces with the material injecting printing technology is an arduous task.

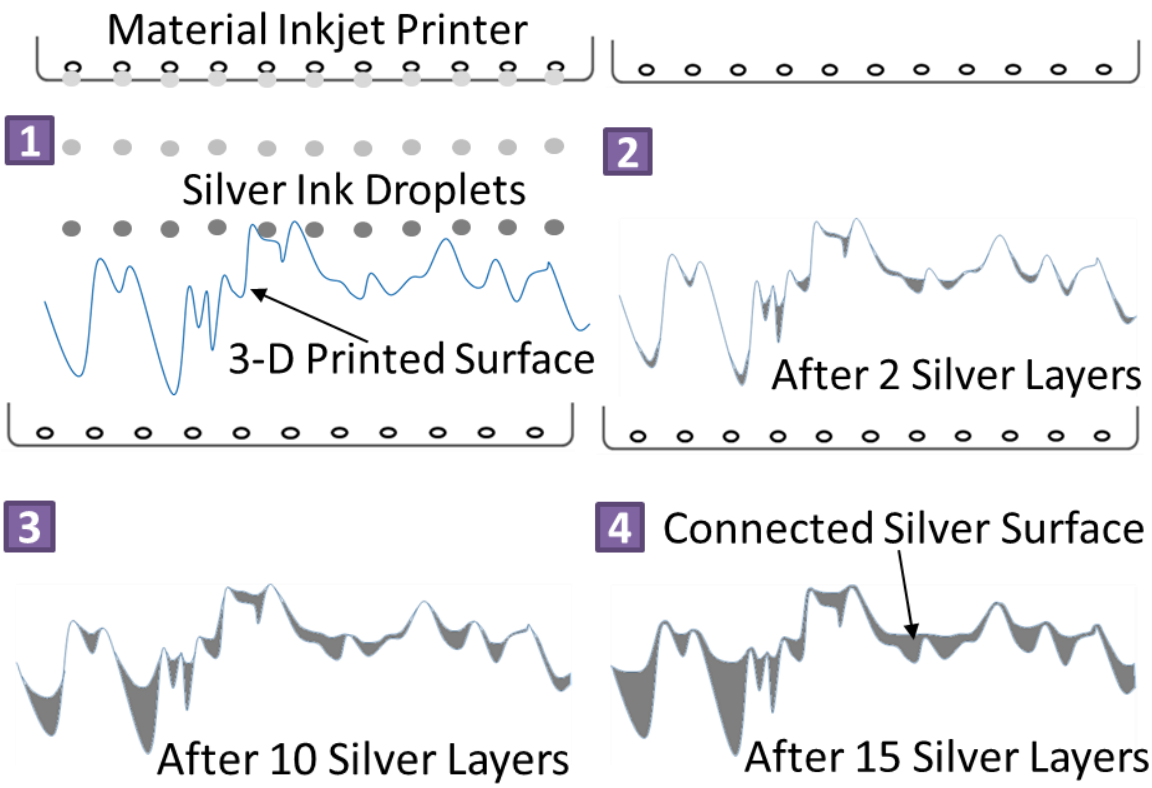

Figure 2.6 Metallization of the 3-D printed substrate using material inkjet printer

Figure 2.6 shows the metallization process of the Verowhite substrate by using material inkjet printing technique. As soon as the silver droplets touch the surface they flow into the depression or the cavities. The discontinuities of the silver ink on the rough 3-D printed substrate increases the resistance to the flow of the electrons, reducing the overall conductivity.

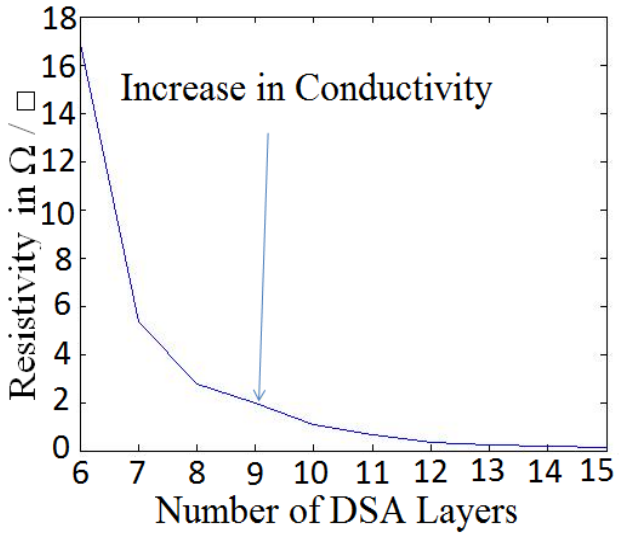

Figure 2.7 Resistivity versus number of DSA layers on 3-D printed substrate

DSA Layers	**Resistivity Ω / □**
6	17
7	5.35
8	2.788
9	1.95
10	1.069
11	0.6428
12	0.366
13	0.24
14	0.179
15	0.157

Table 2.1 DSA deposition layers compared with respective resistivity

Hence, for the initial layers very high resistivity was measured as mentioned in Table 1. Also, the varying skin depth affects the RF conductivity which significantly reduces the radiation efficiency by increasing the material losses. After 15-20 layers of the DSA silver ink deposition, the resistivity was significantly reduced that means the surface cavities of the 3-D printed substrate got filled with the enough conductive silver ink and it forms a conductive layer of the silver ink as explained in Figure 2.6.

CHAPTER III

ADDITIVELY MANUFACTURED ANTENNAS

3.1 Fully Printed Aperture Coupled Patch Antenna

In this section, a fully additively manufactured multilayer aperture-coupled patch antenna operating at the ISM band around 2.45 GHz is demonstrated. For the fabrication of fully printed aperture coupled antenna, 3-D and inkjet printing technique was utilized. This is the first demonstration of the antenna fabrication technique that employs only additive manufacturing techniques to print consecutive conductive and dielectric layers. The metallization of the 3-D printed plastic dielectric layers was performed by inkjet printing layers of conductive ink. To showcase feasibility of this method, multiple layers of Diamine Silver Acetate (DSA) conductive layer were deposited to form a uniform conductive thin layer on the surface of the 3-D printed layers of Verowhite polymer. This Novel fully printed antenna fabrication methodology could enable mass production of low cost printed RF circuits and antennas for a variety of scalable wireless body area sensor network and Internet of Things (IoT) as well as quick component prototyping.

3.1.1 Introduction

The microstrip antennas are widely used in a broad range of military and commercial applications mainly due to their light weight, low profile, and low cost fabrication. Aperture-coupled patch antennas have advantages over conventional patch antennas because aperture coupling eliminates the need for the fabrication of a vias or connections with pins which are necessary for conventional probe-fed patches.

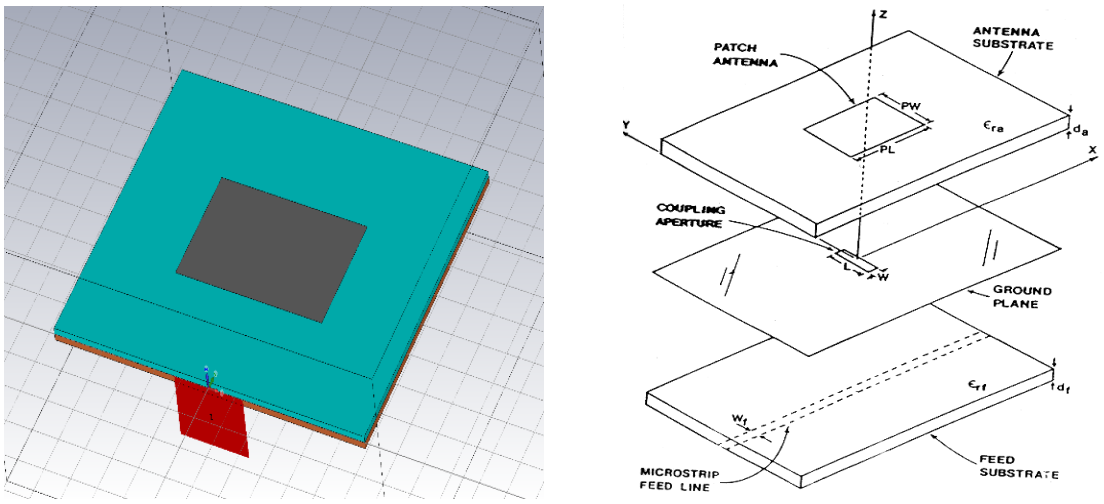

(a) (b)

Figure 3.1 (a) Aperture-coupled patch antenna simulation model (b) Aperture-coupled patch antenna structure [18]

Patch antennas are also key elements for the fabrication of antenna arrays consisting of hundreds or thousands of elements. In aperture-coupled designs, the ground plane is sandwiched in between the feed circuitry and the radiating patch drastically reducing the spurious radiations that commonly corrupts the side lobes level and the polarization of the antenna, due to unintended radiation from the feeding lines.

In section 3.1.2, antenna designing and optimization is discussed. Section 3.1.3 describes our novel fabrication methodology. Section 3.1.4 discusses the influence of the surface smoothness of the 3-D printed dielectric on the conductivity of the inkjet printed metallic layer. Finally, section 3.1.5 shows measured performances of fabricated design.

3.1.2 Multilayer aperture-coupled Antenna Design

The aperture-coupled patch antenna is the type of patch antenna that consists of a five layered structure with the combination of 3 layers of metallic elements and 2 layers of the dielectric substrate. Metallic layers include, feedline, ground plane and radiating patch. The ground plane is sandwiched in between the radiating patch and the feedline and in between each metallic layer there exist substrate material. There exist coupling aperture on the ground plane, usually created under the patch. The coupling factor is between the

radiating patch and the aperture is greatest when the patch is exactly over the aperture, while it decreases significantly as the patch is moved away from the center. The resonant frequency of the antenna is dependent mainly on the length of the patch and slightly on aperture length. Hence, designer gets additional degrees of freedom while designing such antennas.

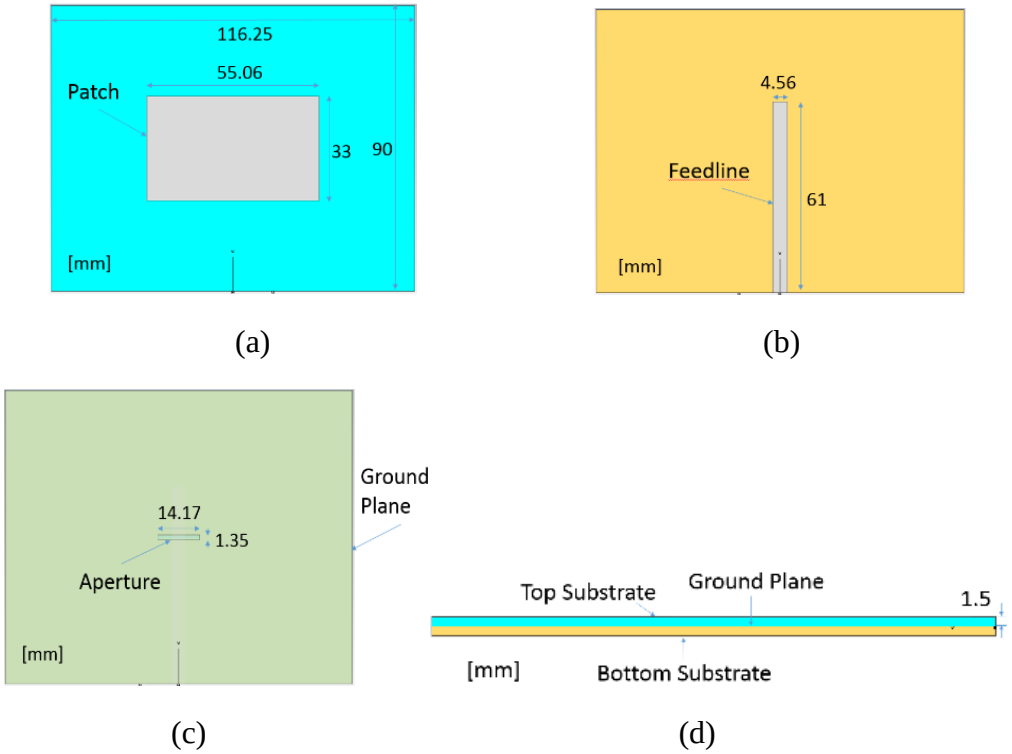

Figure 3.2 Layer-by-layer configuration for modeling simulations (a) Patch on top of the top substrate; (b) Ground Plane and Aperture on top of the bottom substrate; (c) Feedline on bottom of the bottom substrate; (d) Side view

The antenna proposed was designed to operate at 2.45 GHz ISM band to showcase the prototyping of fully printed antenna. Hence the patch and the aperture dimensions were adjusted to tune the operating center frequency of 2.45 GHz and optimized using CST EM simulation tool as shown in Fig. 3. The operating frequency was adjusted by inversely scaling the patch and the aperture dimensions. While designing and optimizing antenna through simulation software, the relative permittivity of the 3-D printed Verowhite material was assumed to be $\varepsilon_r = 2.75$.

3.1.3 Fabrication

In order to demonstrate the novelty and mass production application approach of the proposed multilayer fabrication approach, only additive manufacturing techniques were employed to fabricate this fully printed multilayer antenna design. An Objet Connex 260 3-D printer which employs PolyJet 3-D printing technology, was utilized. It has the accuracy of 15 microns which provides high precision. It is similar to inkjet document printing, but instead of jetting drops of ink onto paper, PolyJet 3-D Printers jets layers of liquid photopolymer onto a build tray and cure them with UV light.

The Dimatix material inkjet printer was used to deposit uniform layers of conductive material. To deposit conductive material diamine silver acetate (DSA) on the 3-D printed substrate uniformly, it was necessary to minimize the surface roughness of the 3-D printed dielectric. This was obtained by optimizing slicing parameters of the 3-D printer though 3-D printing software.

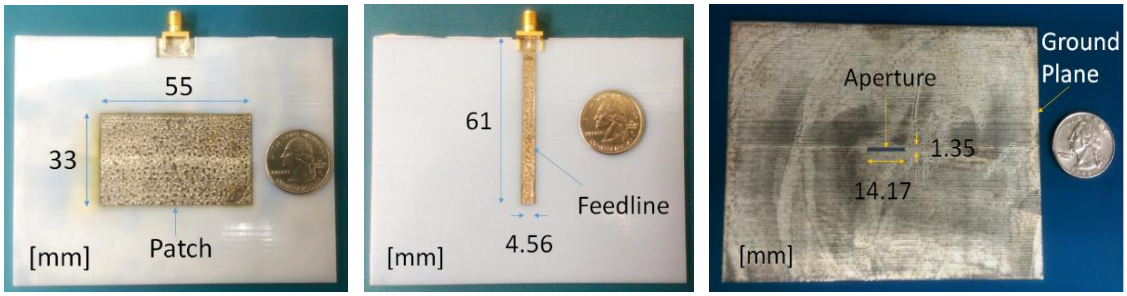

(e) (f) (g)

Figure 3.3 After fabrication (e) Patch on top of the top substrate; (f) Feedline on bottom of the bottom substrate; (g) Ground Plane and Aperture on top of the bottom substrate

First, the bottom substrate layer of Verowhite material of optimized dimensions (e.g. 116.25×90×1.5mm) was 3-D printed. As shown in Fig. 4 (g) the ground plane with the aperture at the center was printed by Dimatix material inkjet printer with an appropriate spacing of 40μm between the printed drops. The number of layers of DSA required to achieve the necessary conductivity was determined experimentally. A feedline was

printed similarly on the lower side of the bottom substrate. It took 15 Layers of DSA to get a conductivity of 0.157 Ω / □.

Once the feedline was printed, one more layer of Verowhite was 3-D printed on the ground plane with a thickness of 1.5mm and a width and length of respectively 116.25mm and 90mm; this is the top substrate of the structure. The patch antenna with optimized dimensions was then inkjet printed on top of the top substrate with a similar method as the used in the fabrication of conductive ground plane and feedline.

3.1.4 Conductivity of DSA on 3-D Printed Substrate

In this section, the importance of the surface smoothness of the 3-D printed substrate on the conductivity of the inkjet printed DSA layers is demonstrated.

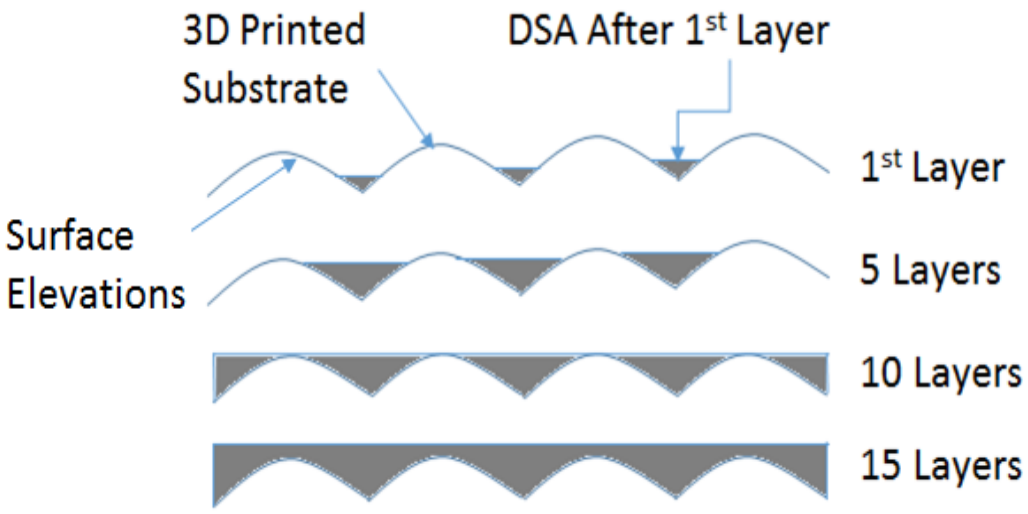

(a)

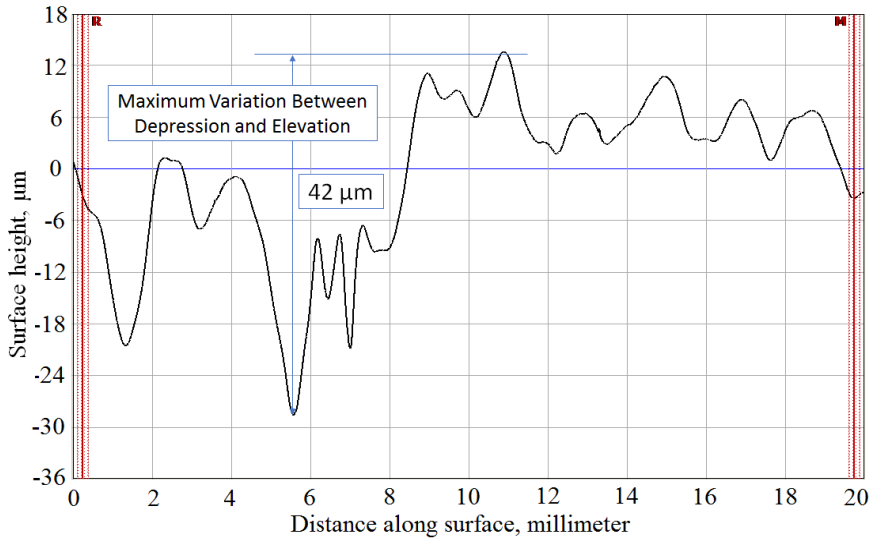

(b)

Figure 3.4 (a)DSA Ink Deposition by a Material Inkjet Printer on 3-D Printed Object (b) Measured Surface Roughness of a 3-D Printed Substrate using a Profilometer

Fig. 5 (a) illustrates the effect of surface roughness on the conductive material inkjet printing on the top of a 3-D printed substrate. Unfortunately, the 3-D printed substrate has periodic as well as random elevations and depressions on its surface. To measure its exact surface roughness, a profilometer was used.

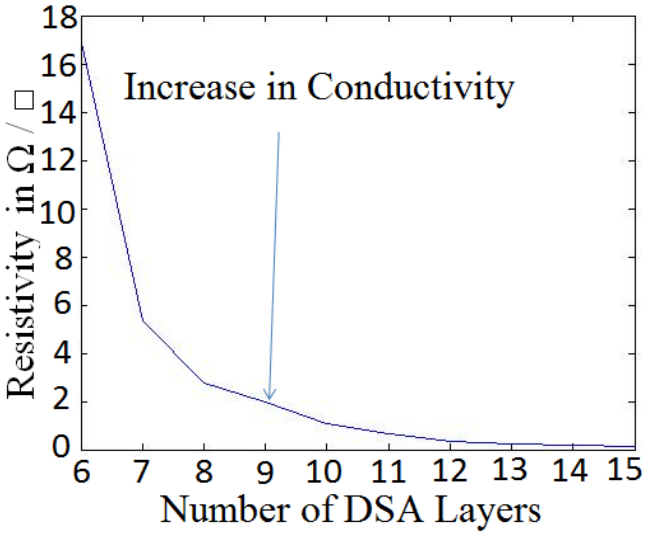

Figure 3.5 Number of Inkjet Printed DSA Layers Vs Resistivity

Fig. 3.4 (b) illustrates the surface roughness of the 3-D printed dielectric substrate, which is varying arbitrarily with a maximum vertical variation of 42um between a depression and an elevation.

DSA Layers	**Resistivity Ω / □**
6	17
7	5.35
8	2.788
9	1.95
10	1.069
11	0.6428
12	0.366
13	0.24
14	0.179
15	0.157

Table 3.1 Number of Inkjet Printed DSA Layers Vs Resistivity

Due to the roughness-related discontinuities, initially up to 10 layers of DSA leads to a low conductive printed film.

After a sufficient number of printed DSA layers - typically larger than 15 - the separated islands of DSA material connects with each other over the whole surface forming a thin conductive layer. This effect can be observed in Figure 3.4 where we can observe initially a sharp and then gradual increase in conductivity with the increasing number of DSA layers.

3.1.5 Results

The antenna characteristics were measured using a Rhode & Schwarz ZVA8 vector network analyzer. A 50-coaxial SMA connector was connected with conductive silver epoxy for measurement purposes.

The simulation and measured S_{11} return loss results of the antenna can be seen in Figure 3.6. The return loss values of the additively manufactured antenna prototype with a good agreement in the resonant frequency value. However, we can see that the losses of the fabricated antenna are quite high.

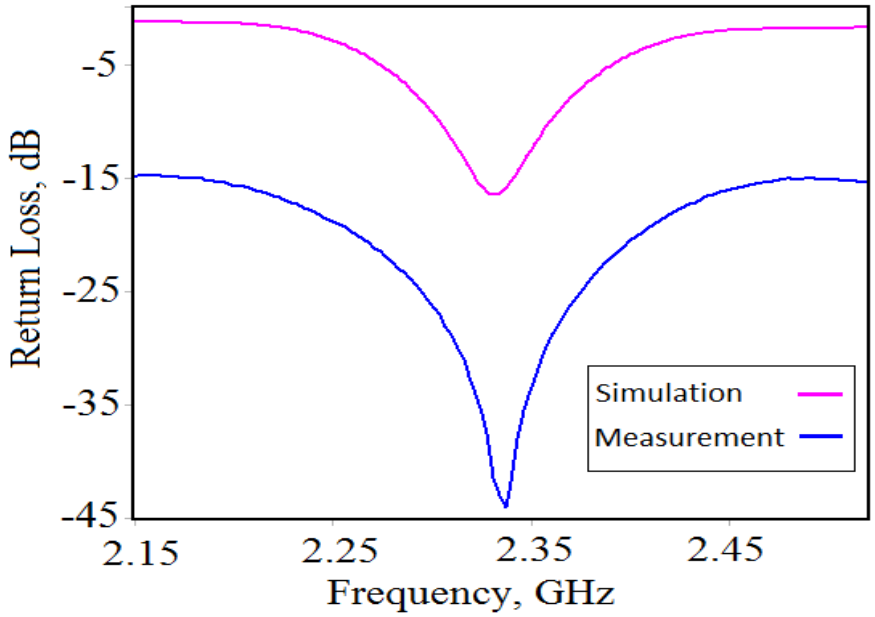

Figure 3.6 S_{11} Return loss

This is most likely due to non-uniformities and gaps in the inkjet printed conductive layers due to the surface roughness of the 3-D printed substrate. We expect that this can be greatly improved by further increasing the number of printed DSA layers.

3.2 3-D Printed Loop Antenna by Flexible NinjaFlex Material for Wearable and IoT Applications

This section introduces a novel 3-D loop antenna on hemi-sphere utilizing the flexible NinjaFlex material for the first time. The proposed antenna can be useful for the flexible, wearable and 3-D electronic packaging applications, such as health monitoring earrings and Internet-of-Things (IoT). Also the proposed configuration was tested for the wireless strain detection application. It could be useful in tactile sensing for the "smart" skin and the flexible electronics [14] applications.

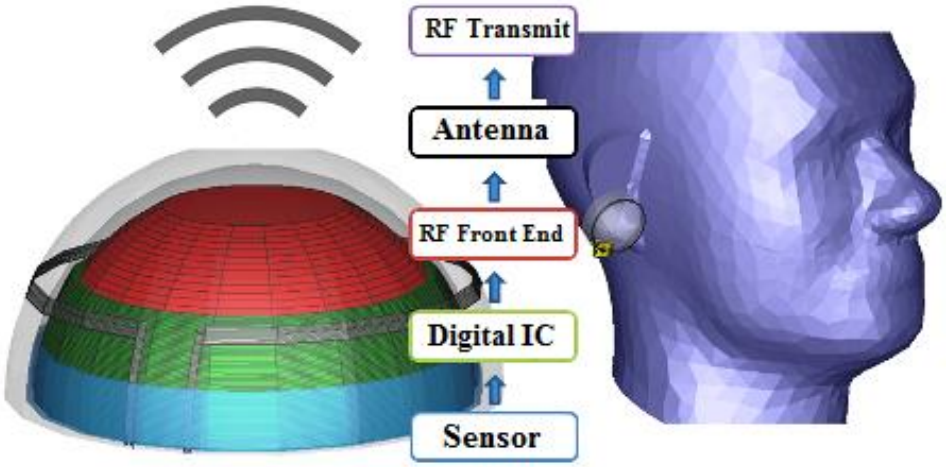

Figure 3.7 1 3D packaging for health monitoring and IoT applications

3.2.1 Design and Modelling

The electrically large circular loop antenna topology was chosen because of its large front and back lobes effectively synthesize a nearly omni-directional radiation pattern. This could be very useful in the "health monitoring earrings" applications enabling an almost non-intermittent connection to nearby wireless networks. The detailed loop antenna design procedure can be found in [26]. Without loss of generality, the optimized parameters of the 3D fabricated prototype were chosen to be equal to $k\rho = C/\lambda = 0.896$ at 2.4 GHz and $\Omega = 2 \ln(2\pi\rho/b) = 5.3675$, where k = wavenumber, ρ = radius of loop, C =

Circumference of the loop, λ = wavelength, b = metal trace thickness. The thickness of the substrate was chosen to be 1.5mm for SMA connector to get a firm grip while feeding the loop.

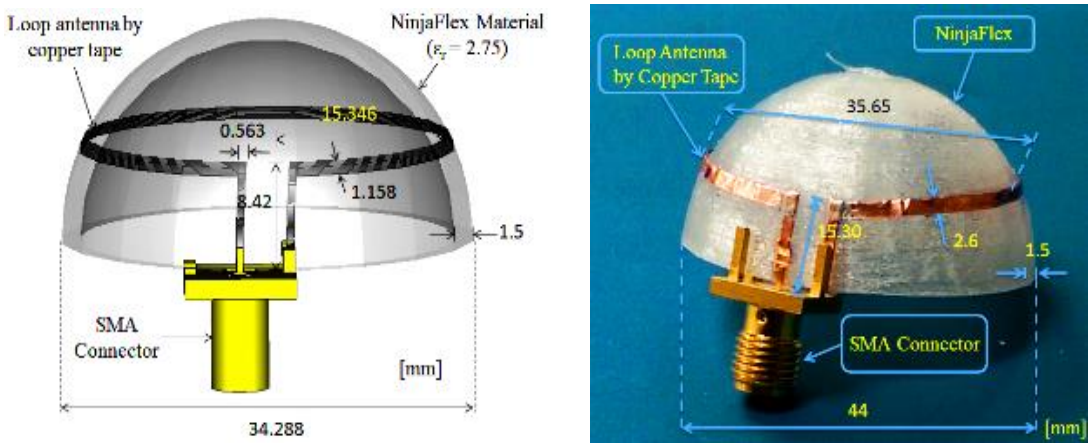

Figure 3.8 a) Optimized simulation model of loop antenna in CST Microwave Studio, b) Fabricated 3D loop antenna with the dimensions after tuning

The relation between the loop radius ρ, hemi-sphere radius r and height of the loop from ground z was found by the spherical to cylindrical coordinate system conversion formula. It gave the value of r when ρ was chosen from the designing method mentioned in [26] and the z was optimized in such a way that feeding line would make least potential radiation loss.

3.2.2 3-D Printing and Ninjaflex Material

NinjaFlex filament was introduced by Fenner Drives Inc. in 2014. It is a type of thermoplastic elastomers, made up of combinations of the thermoplastic and the rubber, which provides the flexible properties to the material. It is very important for the effective 3-D printing of this material to fully investigate and optimize the melting temperature, the extrusion width, the layer height and the print speed to ensure smooth and the near-hermetic designs. These parameters were optimized in the Slicer software. The extrusion temperature was set to the melting temperature of the NinjaFlex at 2300C. The extrusion width was optimized to 0.5mm to realize the hermetic 3-D model. Also,

the layer height was optimized to 200μm to have a smooth flow of the extruding material; this specification typically decides the thickness of each layer as well printing time. The Ninjaflex substrate was 3-D printed by Hyrel 3-D printer and then the copper tape of the optimized loop antenna size was glued on the top of the 3-D hemispherical support. The connection between the 50 Ω-coaxial SMA connector and the loop antenna terminals was realized utilizing a silver epoxy.

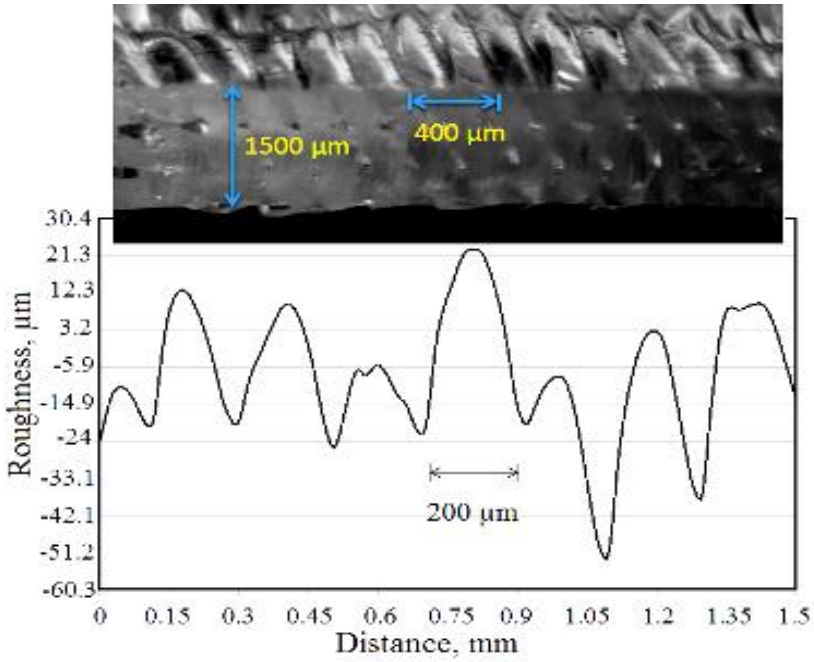

Figure 3.9 Profilometer measurement compared with microscopic cross section of NinjaFlex Sample

The surface roughness of the NinjaFlex material was measured by KLA Tencor Alpha-Step D-500 Stylus profilometer in order to have some preliminary estimates of the losses at high frequencies. The surface roughness information is useful to estimate losses at higher frequencies due to the surface roughness. The microscopic cross section image was taken through AmScope Microscope. The 3D printed substrate has periodic as well as random elevations and depressions on its surface with the maximum difference of 74μm between the tallest elevation and the deepest depression measured. 200μm width of the elevation indicates the layer height.

3.2.3 Results

A. Return Loss S_{11}

The antenna characteristics were measured using a Rhode & Schwarz ZVA8 vector network analyzer in the frequency range of 2–3 GHz.

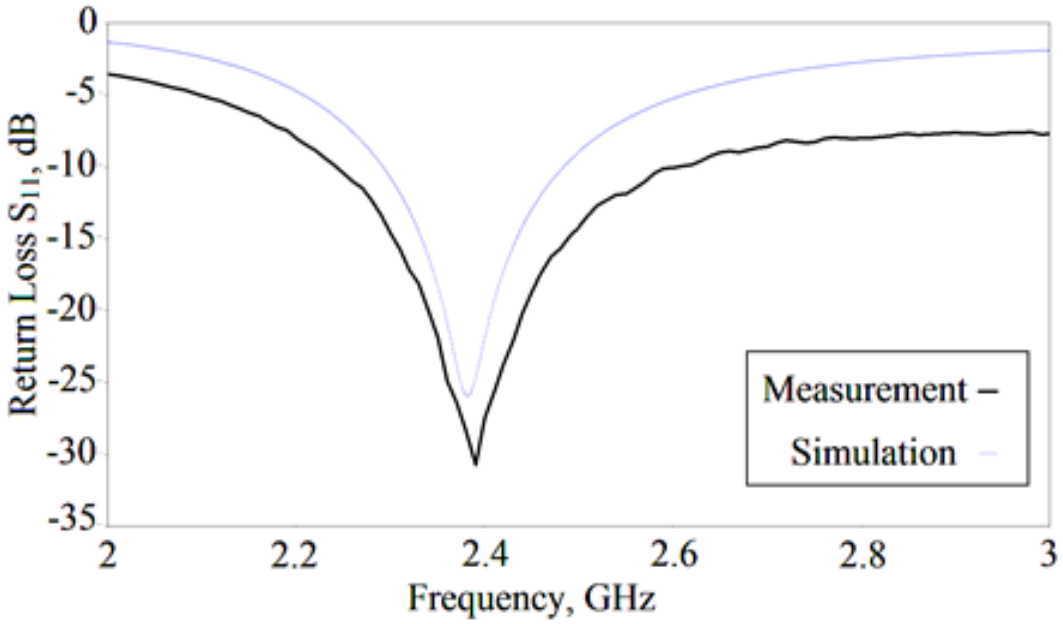

Figure 3.10 Return loss S_{11} of the loop antenna

Fig. 5 shows good agreement between measured and simulated return loss S_{11} results of the 3D loop antenna. The antenna was tuned to work in the bandwidth of 2.32 to 2.5 GHz band covering 2.4-2.5 GHz ISM band. However, losses can be seen at the higher frequencies due to the surface roughness of 3D printed NinjaFlex.

B. Specific Absorption Rate (SAR) Measurement

Proposed antenna packaging was designed for the wearable applications such as the health monitoring earrings. Hence, it was essential to make the antenna design in such a way that it will radiate within the standard safely limitations when placed on user's body [29], [30]. SAR value depends on radiation pattern of the antenna and applied power to the antenna. Hence the proposed antenna parameters were optimized to get a null towards head when placed on the ear of the human head replicating model. In CST MW studio,

the SMA connector, the waveguide port and the discrete port were used to excite the loop antenna and then the SAR measurements were taken to understand the effect of power and excitation method variation on the SAR values. FCC and CENELEC assign a limit on the SAR in the US and Europe respectively [33], [34].

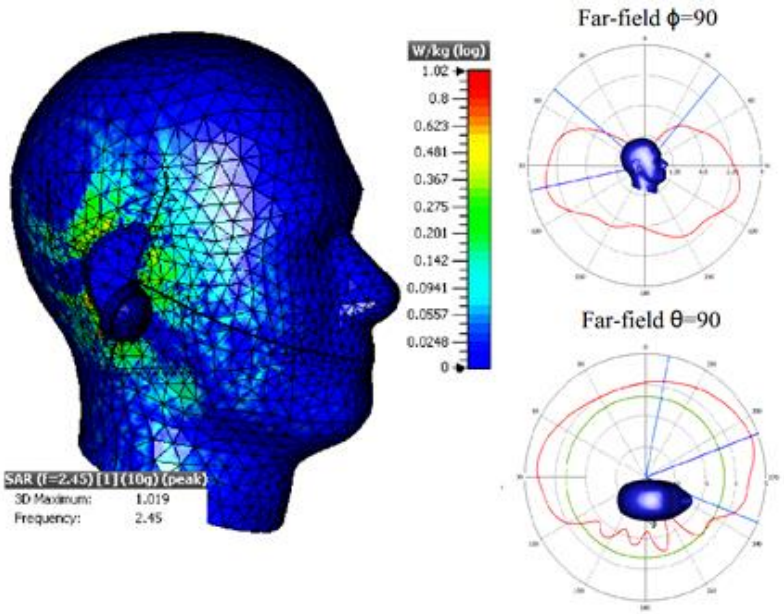

Figure 3.11 SAR Measured in CST Microwave studio and radiation pattern while 3D loop antenna presents on the ear of the user

In the simulations, the specific anthropomorphic mannequin (SAM) phantom head model was utilized. It was provided by CST Microwave Studio. The outer shell of the head had a fixed relative permittivity of $\varepsilon_r = 5$ with an electrical conductivity of 0.01252 S/m [30] and the head simulating liquid had the relative permittivity of $\varepsilon_r = 42$ with an electrical conductivity of 0.99 S/m. The following table indicates the effect of different excitation methods on SAR values.

Type of Excitation	Avg. mass 1gm FCC Std., W/kg	Avg. mass 10gm CENELEC Std., W/kg
Limitations	1.6	2
SMA	1.45	1.02

Table 3.2 SAR values w.r.t. different types of excitation methods

C. Strain Sensor

Flexible properties of NinjaFlex make it an epitome of wireless strain sensor. Hence variations over return loss S_{11} with respect to the amount of deformation/strain were taken. The change in shape of the antenna affects effective capacitance across the loop configuration to change, eventually changing the tuning frequency of the configuration.

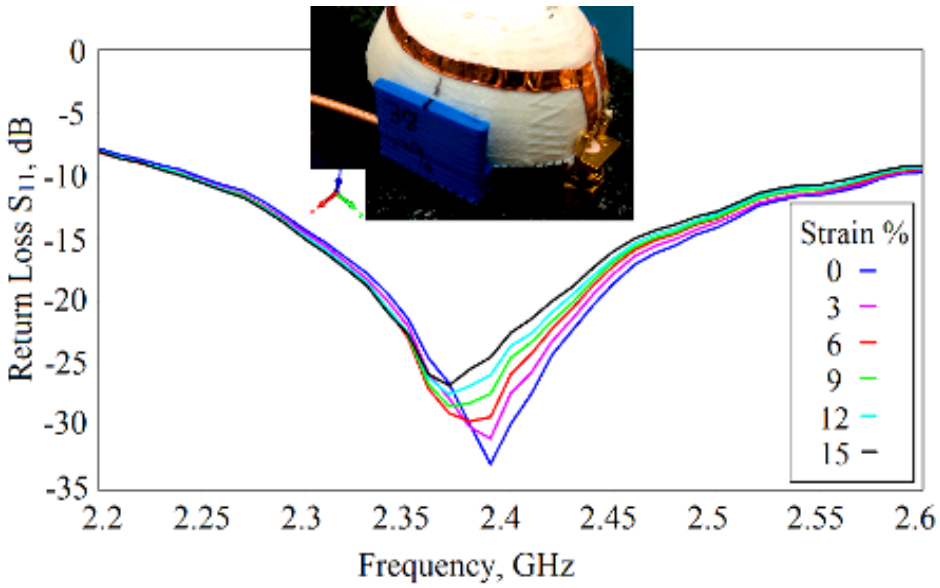

Figure 3.12 Measured return loss of loop antenna under different strain percentage

It was crucial to make an assembly to obtain persistent values of the deformation over same applied force without using the standard metallic mechanical tester. Hence 3D printed slots of the different dimensions that would apply strain of 0, 3, 6..15% on the sensor was fabricated. Same position of the sensor was maintained while taking 4 cycles

of the strain measurements to ensure repeatability and reliability of the sensor. There were no signs of any physical damage after stretching, twisting and folding it multiple times.

CHAPTER IV

COMPACT PLANAR RECTANGULAR SPIRAL ANTENNA FOR IOT APPLICATION

4.1 Introduction

Electronic systems for IoT applications are swarming the consumer and industrial markets with the aim of sensing, computing and connecting all things within reach. Ever compacting electronic systems highly demand the compact passive components. It is the challenge for the engineers to feed the hunger of the miniaturization of the wavelength dependent passive components. The proposed antenna design demonstrates the efficient use of the electromagnetics fundamentals to reduce the size of the electrical small antennas (ESA). The designing, modelling and testing of the compact planar rectangular spiral antenna operating at 433.9 MHz with the 5.81 MHz bandwidth for the FR-4 substrate material is explained. The size was reduced by using high dielectric constant Rogers material to 44×20 mm^2. The antenna had omnidirectional radiation pattern apt for the most of the IoT applications.

4.2 The antenna design

The designed planar rectangular spiral antenna is electrically small antenna with the maximum length of 0.073λ. The rectangular spiral antenna is fed with the 50Ω microstrip line. The spiral antenna has one and a half turns with the inner end is connected to the patch acting as a capacitive load. The capacitive load increases the electrical length of the antenna while reducing the physical length of the antenna. This also increases the effective aperture of the antenna improving the bandwidth as well as the radiation efficiency. But such arrangement increases the overall capacitance of the system which reduces the matching efficiency with the 50Ω microstrip feed line. Hence the inductive inverted F element has been added at the upper end of the spiral structure as shown in

Figure 4.1 to compensate the additional capacitance in the system. That leads the capacitive components of the impedance to cancel the inductive components producing the resistive response of the antenna which is responsible for the far field radiation.

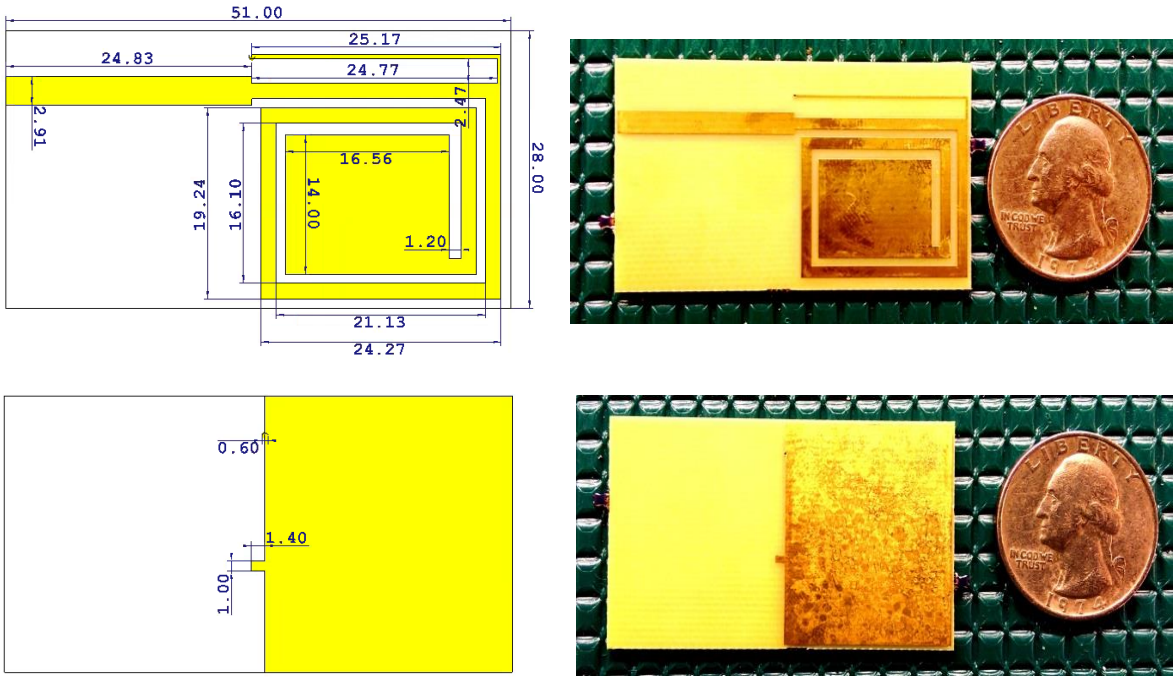

Figure 4.1 Planar rectangular spiral antenna simulated design and fabricated prototype

The antenna was modified from 3 different antenna concepts to reduce the length and to achieve the tuning namely monopole patch antenna, rectangular spiral antenna and inverted F antenna. If you look from the feeding side, the antenna works like a monopole patch antenna with the 50Ω microstrip line feeding the rectangular spiral antenna acting as a modified version of the monopole patch antenna. The planar rectangular spiral antenna concepts were used to reduce the structure length and to improve the low frequency tuning which was further modified with the capacitive loading at the center. If you look from the right upper corner of the top view of the antenna, the structure looks like the modified version of the inverted F antenna with the inductive inverted F element connected to the capacitive ground structure. We have modified the ground structure present in the conventional inverted F antenna with the rectangular spiral antenna. The inverted F antenna itself is the modified version of the slot antenna. Additional capacitive

stub was added to further control the reactance of the antenna and achieve the fine tuning in the desired bandwidth.

4.3 Simulation and optimization

The antenna was simulated and optimized in the CST Microwave Studio software. The antenna was tuned by addition or subtraction of the reactance from the reactive elements of the antenna and the dimensions of the elements.

Following are the knobs available for the antenna designer to tune the antenna at the desired frequency: The length and width of the spiral elements, the perimeter of the capacitive patch, the length and width of the inverted F element and the capacitive stub connecting the ground plane.

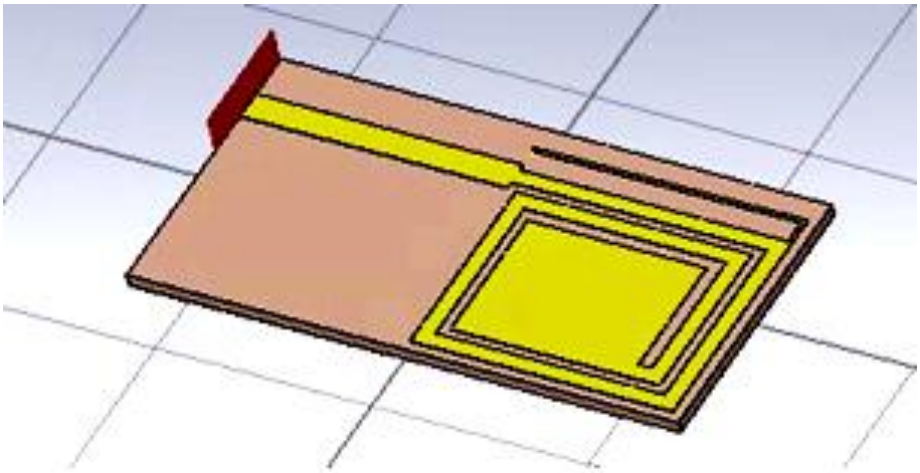

Figure 4.2 Simulated model in CST microwave studio

The perimeter of the capacitive patch attached to the inner end of the spiral antenna is the dominant contributor for the overall capacitance in the antenna system. Also the dimensions of the patch significantly affect the bandwidth of the antenna. At the desired frequency band this capacitance was compensated by tuning the width of the inductive inverted F element attached to the antenna. The width of the inverted F element is inversely proportional to the amount of inductance generated. This is the dominant contributor to the overall inductance in the system. The antenna tuning was mainly achieved with these knobs and later the fine tuning was achieved with the capacitive stub

present on the other side connected to the ground. Since the frequency shift by the change in the dimensions of the stub is comparatively small. In the simulation, the waveguide port was connected to the 50Ω microstrip feedline to imitate the coaxial SMA connector producing the TEM wave along the feedline.

The simulation was performed on the FR-4, Rogers RO 4360G2 and RO 3006. FR-4 has the dielectric constant 4.15 and the loss tangent 0.02 while the Rogers materials utilized have 6.15 dielectric constant. The high dielectric constant reduces the overall dimensions of the antenna. RO 3006 is comparatively high performance material with very low material losses as the loss tangent is 0.002. RO 4360G2 is the more economical option compared to RO 3006 and possess low dielectric losses than FR-4 due to low loss tangent 0.0038.

4.4 Fabrication

The fabrication was done with LPKF ProtoMate S42 milling machine of resolution 7.5µm. The fabrication was done by using FR-4, RO 4360G2 and RO 3006 substrate materials with the simulated and the optimized design.

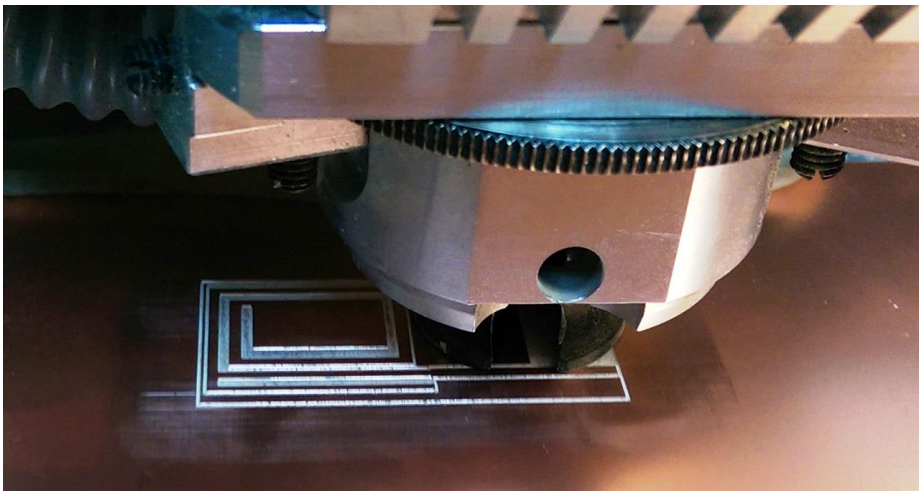

(a)

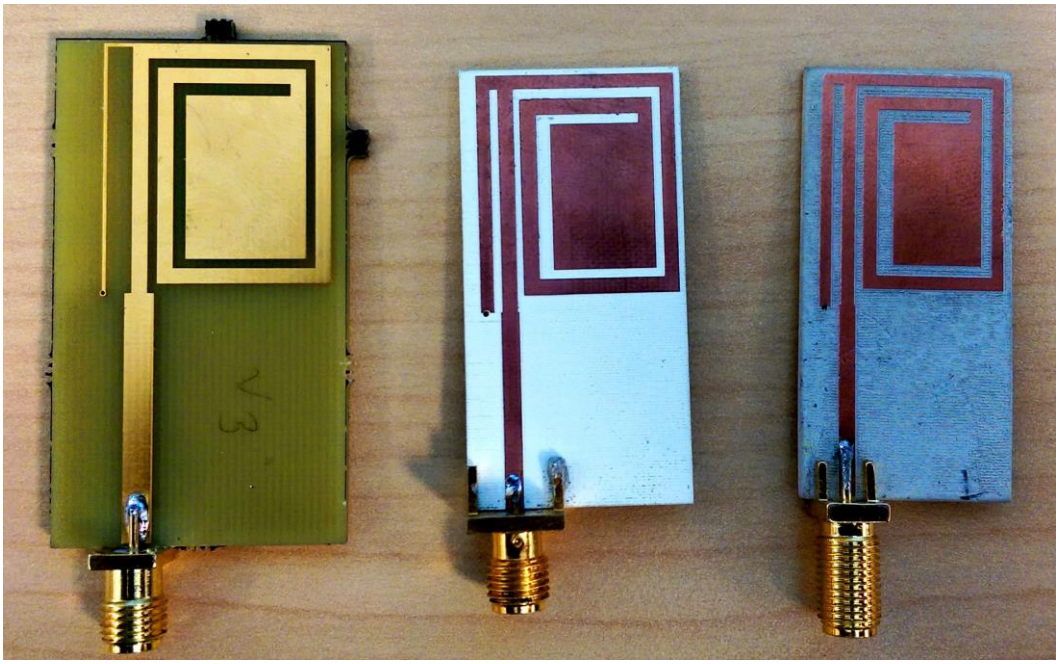

(b)

Figure 4.3 (a) Fabrication using ProtoMate S42 milling machine (b) Fabricated prototypes using FR-4, RO 4360G2 and RO 3006 substrate materials

The Rogers materials were utilized for the high dielectric constant and low loss tangent. The RO 3006 is high performance soft material while the RO 4360G2 is comparatively economic option with high durability. The FR-4 is the cheapest among the options however it lacks in the performance due to high material losses.

4.5 Results

4.5.1 Return Loss S_{11}

The antenna characteristics were measured using a Rhode & Schwarz ZVA8 vector network analyzer. The VNA was calibrated to eliminate the cable and connector losses in the frequency range of 400-500 MHz.

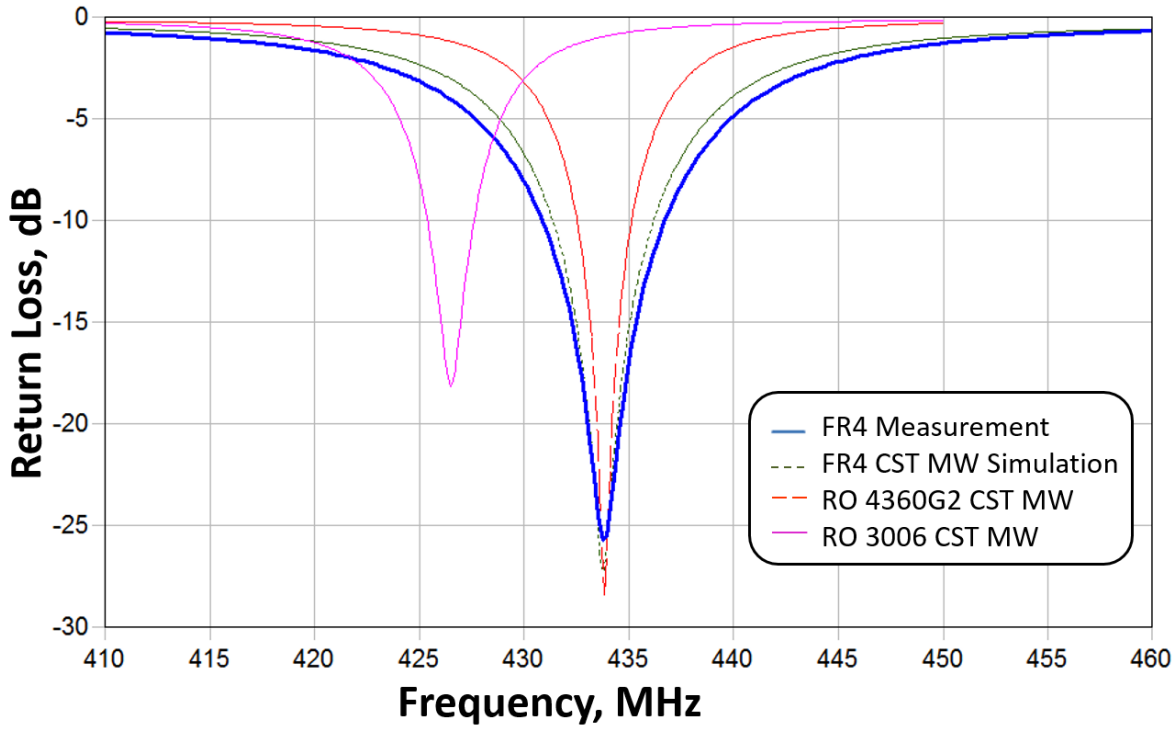

Figure 4.4 Return loss of the antenna measured with R&S VA8 VNA and CST simulation software

Figure 4.4 shows the good agreement of the simulation and measured return loss. The measured return loss shows tuning with the magnitude of -25dB at the center frequency of 433.9MHz with the 6MHz bandwidth for FR-4 substrate material. The antenna on the RO 4360G2 substrate material was tuned at the 433.9 MHz ISM center frequency with the bandwidth of 2.6 MHz in the CST MW Studio software. The antenna design was also tuned for the RO 3006 substrate material at 426.5MHz with the bandwidth of 2.2 MHz.

4.5.2 Q-Factor

The planar rectangular spiral antenna changes the bandwidth mainly due to the material dielectric properties and the thickness of the substrate that eventually results in different Q-factor design options. The bandwidth can also be varied by changing the antenna surface area. The antenna was designed considering the diverse IoT applications and the dielectrically adverse surrounding environments. When an antenna is placed on the high dielectric lossy materials, the reactance of the antenna changes which shifts the tuning

frequency. The simulated and fabricated design achieved the highest bandwidth with the FR-4 substrate material. Such antenna designs are important for the dielectrically adverse conditions to compensate the frequency shift due to the surrounding material and to maintain adequate antenna efficiency without being affected largely by the impedance mismatching.

Substrate Material	Q-Factor	Bandwidth (MHz)	Substrate Thickness (mm)	Dielectric Constant (ε_r)
FR-4	74.65	5.81	1.5	4.15
RO 4360G2	166.85	2.6	1.5	6.15
RO 3006	193.864	2.2	1.28	6.15

Table 4.1 Q-Factor for different substrate used

Table 4.1 shows that the dielectric constant and the thickness of the substrate affect the Q-factor the most. High dielectric constant reduces the size of the antenna in the expense of the bandwidth. If the antenna is tuned at the frequency considering the frequency shift due to surrounding environment prior to the deployment, then it is advisable to use high Q-factor antennas. Sometimes it's an antenna designer's call to choose the Q-factor from the available substrate material options.

4.5.3 Smith Chart

The antenna impedance matching was achieved in a such way to that the input impedance circle was near the constant resistance circle. Hence any mismatch due to dielectric environment does not cause the significant resistance change of the antenna. Figure 4.5 shows the measured smith chart taken with the VNA connecting the antenna with the FR-4 substrate.

The inductive and capacitive elements dimensions were the key of producing resistive response of the antenna at the tuning frequency.

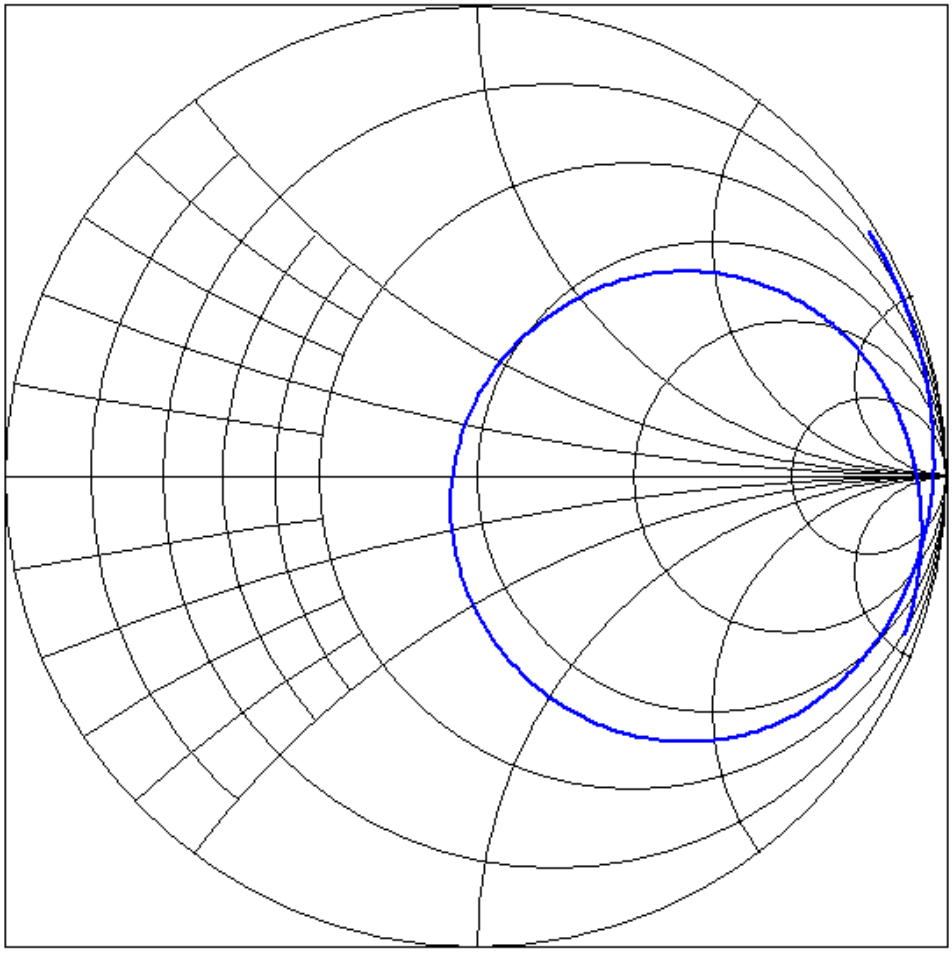

Figure 4.5 Measured antenna smith chart with R&S VA8 VNA

4.5.4 Radiation Pattern

The radiation pattern of the simulated antenna was near omni-directional. The omni directionality of the radiation properties of the antenna was important for the most of the IoT applications.

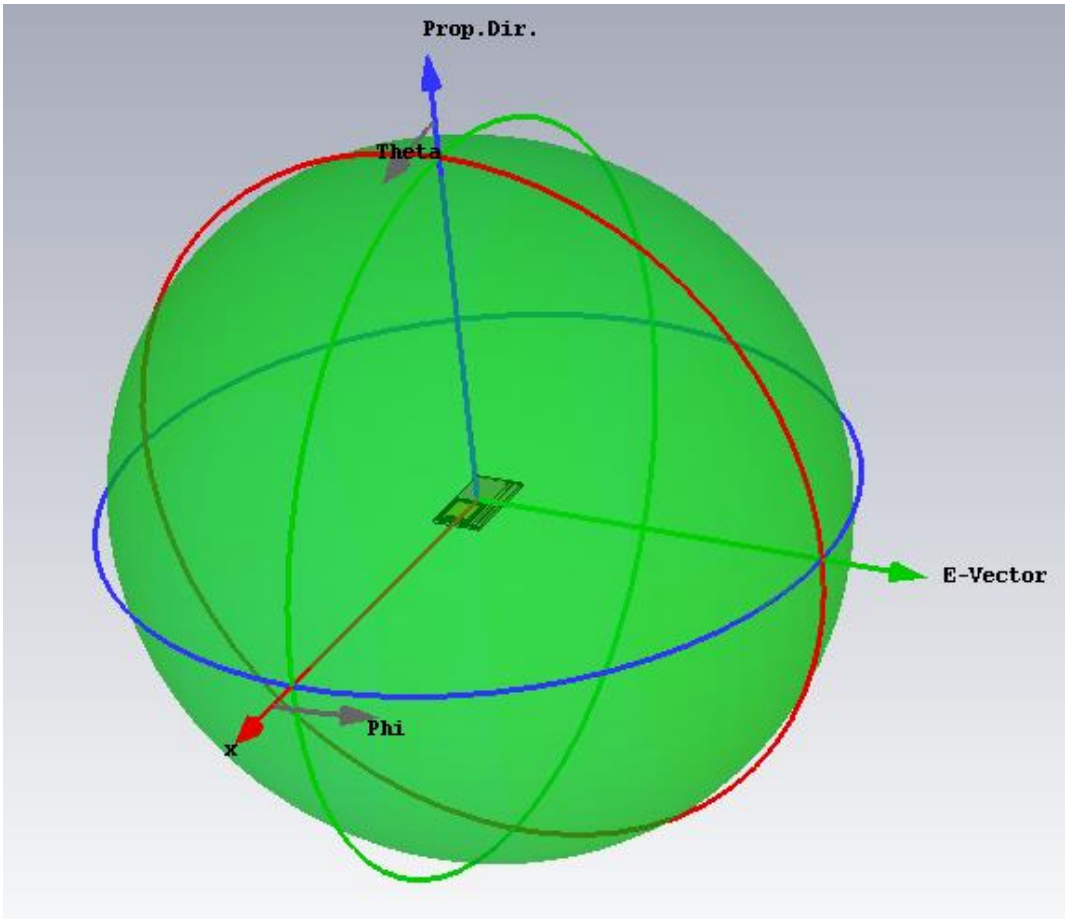

(a)

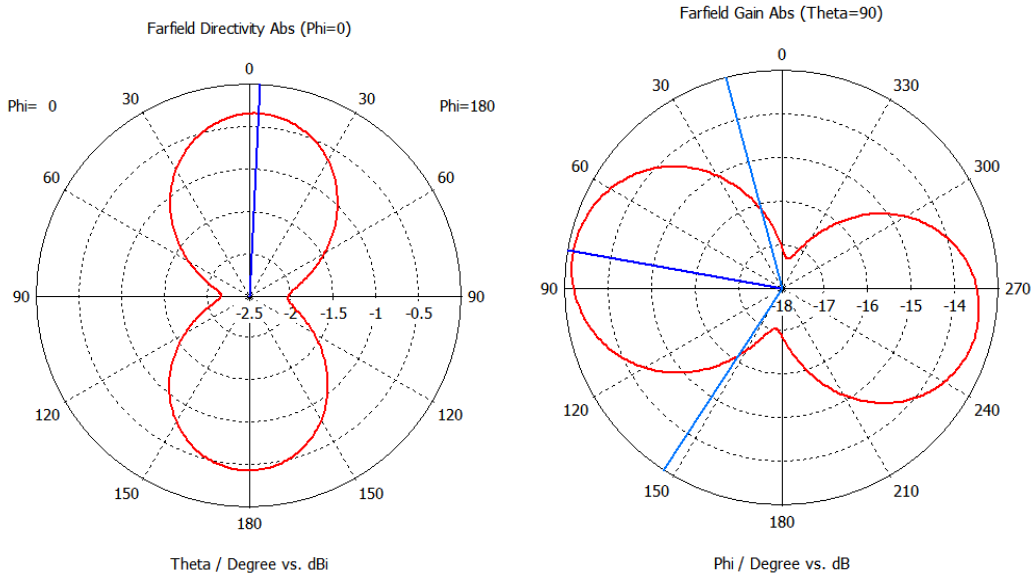

(b) (c)

Figure 4.6 (a) 3-D radiation pattern (b) 2-D radiation pattern of Phi-cut at 0^0 (c) 2-D radiation pattern of Theta-cut at 90^0

4.6 Radiation Efficiency Measurement by Wheeler Cap Method

The antenna gain of any antenna depends on two factors, first is the directivity and second is the antenna efficiency. Most of the electrical antennas are omnidirectional by nature. Also in almost all IoT applications in which the sensing devices are moving, require the omnidirectional radiation properties. Hence the parameter of interest is the antenna efficiency. Antenna efficiency depends on two factors, the matching efficiency and the radiation efficiency. Hence in the early stages of the antenna designing the efforts were put to optimize the matching with the 50Ω reference. The peak return loss -25 dB means that more than 99% of the power applied to the antenna was received by the antenna. Hence the next important parameter is the radiation efficiency. Radiation efficiency takes into account all the material losses from the dielectric substrate and the copper.

Radiation efficiency can be defined by the following formula:

$$\text{Radiation Efficiency } (\eta) = \frac{P_{RAD}}{P_{IN}}$$

$$= \frac{P_{RAD}}{P_{RAD} + P_{LOSS}} = \frac{I^2R_{RAD}}{I^2R_{RAD} + I^2R_{LOSS}} = \frac{R_{RAD}}{R_{RAD} + R_{LOSS}}$$

Where P_{RAD} = Radiated power by the AUT

P_{LOSS} = Loss power of the AUT

R_{RAD} = Radiation resistance

R_{LOSS} = Loss resistance

The above equation creates basic understanding towards the radiation efficiency. Derived equation tells that the power radiated by the antenna can be represented by the equivalent resistances or the real part of the input impedance of the antenna.

Some part of the input power is radiated in the environment and remaining is the power loss. The radiated power is nothing but the resistive energy responsible for the far-field radiation or the long distance communication. The loss power represents the stored energy and the dielectric losses. These two types of power values are required to obtain the radiation efficiency. Wheeler discovered that the radiated power and the loss power can be extracted from the input impedance of the antenna. He discovered that if we place the conductive shield of radius $\lambda/2\pi$, the radian distance around the antenna we can obtain the loss power and eventually we can find the radiation efficiency. For electrically small antennas $\lambda/2\pi$ is the boundary between the near-field and far-field region. By placing the Wheeler cap of radius $\lambda/2\pi$ we can isolate near-field from the far-field.

The real part of the input impedance of the antenna is the addition of two components, radiation resistance (R_{RAD}) and loss resistance (R_{LOSS}). Here, the R_{RAD} is proportional to the radiated power and the R_{LOSS} is proportional to the loss power. When the wheeler cap is placed on the antenna the real part of the input impedance is equal to the R_{LOSS}. Hence the equation can be modified as follows:

$$\text{Radiation Efficiency } (\eta) = \frac{P_{RAD}}{P_{IN}} = \frac{R_{RAD}}{R_{RAD} + R_{LOSS}} = \frac{R_{AIR} - R_{CAP}}{R_{AIR}}$$

Where R_{AIR} = Real part of the input impedance in air

$= R_{RAD} + R_{LOSS}$

R_{CAP} = Real part of the input impedance in Wheeler cap

$= R_{LOSS}$

But this equation is only true for the antenna whose equivalent circuit representation is series RLC resonance circuit. However, most of the patch antenna structures represent parallel RLC resonance circuit. The way to check whether the AUT is acting like a series RLC or parallel RLC resonance circuit is to compare the R_{AIR} and R_{CAP} values. If the $R_{AIR} > R_{CAP}$ then the AUT is acting like a series RLC and if the $R_{AIR} < R_{CAP}$ then the AUT is acting like a parallel RLC.

The proposed antenna input resistance increases after placing the wheeler cap on it as shown in Figure 4.7. Hence the planar rectangular spiral antenna is acting like a parallel RLC circuit. Hence the modification in the mentioned formula is needed which is as follows:

$$\text{Radiation Efficiency } (\eta) = \frac{P_{RAD}}{P_{IN}} = \frac{G_{AIR} - G_{CAP}}{G_{AIR}}$$

Where G_{AIR} = Input conductance of the AUT in air

G_{CAP} = Input conductance of the AUT in Wheeler cap

Before the Wheeler cap construction, different arrangements were verified using the CST MW studio software. The hemi-sphere cap with the ground plate was the efficient and the economical way to measure the radiation efficiency.

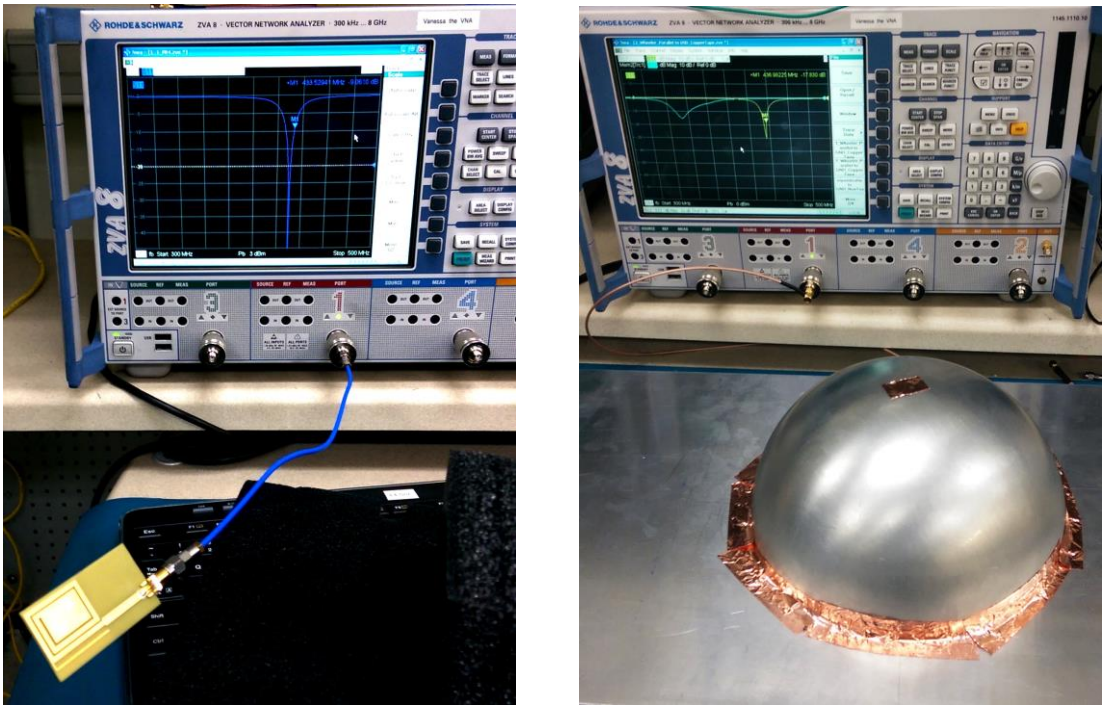

Figure 4.7 S_{11} Return loss measured in air and Wheeler cap

The measurements were performed in free space and in the Wheeler cap of radius $\lambda/2\pi$. The magnitude of the input resistance was varied between the measurements in the free space and in the Wheeler cap. For the measurements to be correct the input resistance values should be used by keeping the fundamental mode of the resonance frequency aligned at the same frequency for the two measurements. That means we have two sets of input resistance values in the desired bandwidth measured one in the air and other in the Wheeler cap, but the tuning frequency shifts in the wheeler cap due reactance from the conductive surrounding. The resonance frequency of the fundamental mode means the frequency at which the resistance of the input impedance is maximum and the reactance is equal to the sum of the average of the maxima and the minima in the desired bandwidth. Ideally, the reactance should be zero. Hence to obtain correct radiation efficiency the two measurements should have the same resonance frequency of the fundamental mode.

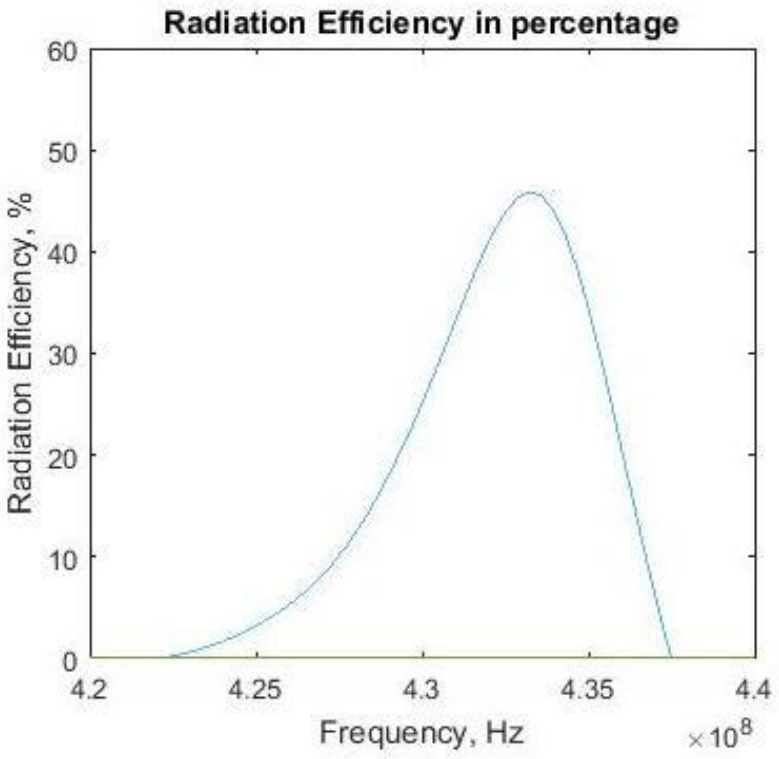

(a)

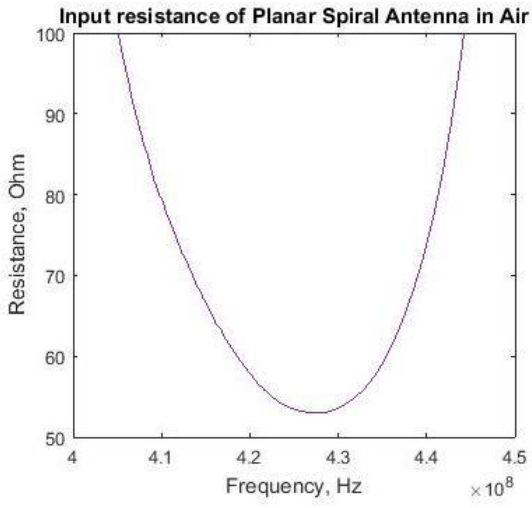

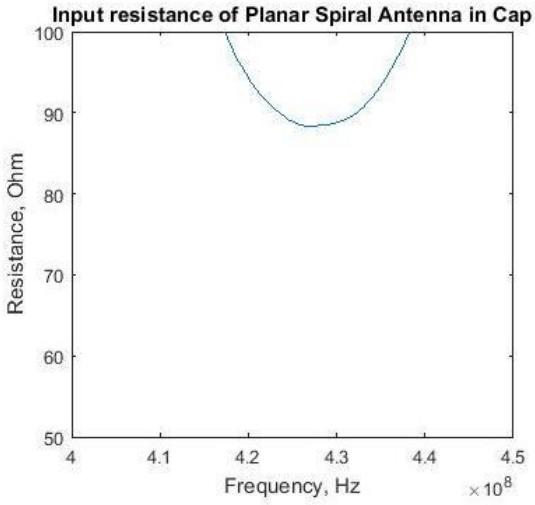

(b) (c)

Figure 4.8 (a) Calculated radiation efficiency (b) input resistance in air (c) input resistance in Wheeler cap

Hence, the Wheeler cap measurement was shifted along frequency axis to match with the resonance frequency of the fundamental mode of the measurements taken in the air. The

post processing of the data to was performed in MATLAB. Figure 4.7 shows the calculated radiation efficiency. The result has the expected nature of the radiation efficiency but there exist some errors in the magnitude. The possible errors could be due to the cavity mode effect generated inside the wheeler cap or the error in the antenna circuit model that needs to be modified over the simple parallel RLC circuit.

CHAPTER V

CONCLUSION

The proposed work demonstrates the antenna components for IoT, compact electronics and wearables using different ways of fabrication such as additive material inkjet printing and 3-D printing as well as the conventional subtractive milling machine fabrication technique. The additively manufactured antennas signify the feasibility of the fully printed antennas and passive components for the new way of electronics packaging. The work is a proof-of-concept demonstration of modern 3-D printing that includes cheap and widely utilized FDM 3-D printing and the high precision and resolution PolyJet 3-D printing technique for the fabrication of RF passive components. The unconventional issue of the surface roughness was discussed. The problem can be resolved with the different curing processes such as SU-8 curing in the future. The efficient way of miniaturization of the electrically small antennas was discussed and a compact design of dimensions 44×20 mm^2 with a good matching at the 433.9MHz ISM band with different materials was achieved. The cheap and accurate way of measuring radiation efficiency was investigated and successfully tested for the rectangular planar spiral antenna. The proposed work could be useful for the ever compacting electronic systems for the IoT and wearable devices.

REFERENCES

[1] Kevin Bullis, "Additive manufacturing is reshaping aviation," in Material News, Feb 2015 [Online] Available: http://www.technologyreview.com/news/534726/additive-manufacturing-is-reshaping-aviation/.

[2] Mike Orcutt. (2015, June). *Could This Machine Push 3-D Printing into the Manufacturing Big Leagues?* [Online]. Available FTP: http://www.technologyreview.com/news/538906/could-this-machine-push-3-d-printing-into-the-manufacturing-big-leagues/

[3] R. Tummala, "SoP: What Is It and Why? A New Microsystem-Integration Technology Paradigm—Moore's Law for System Integration of Miniaturized Convergent Systems of the Next Decade," *IEEE Trans. Adv. Packag.*, vol. 27, no. 2, May 2004, pp. 241-249.

[4] Sung Kyu Lim, "Physical Design for 3D System on Package," *IEEE Des. Test Comput.*, vol. 22 , Issue. 6, pp. 532-539.

[5] "Technology," [Online] Available: http://www.athenis3d.eu/technology.php

[6] Graham Pitcher. (2009, June). *Good things in small packages* [Online]. Available FTP: http://www.newelectronics.co.uk/electronics-technology/good-things-in-small-packages/18879/

[7] A. Pizzagalli, "3D technology applications market trends & key challenges," *Advanced Semiconductor Manufacturing Conf. (ASMC)*, May 2014, pp. 78-81.

[8] Markforged [Online]. Available FTP: https://markforged.com/materials/

[9] Asiga [Online]. Available FTP: https://www.asiga.com/products/materials/

[10] K. A. Nate, M. Tentzeris, "A Fully Printed Multilayer Aperture-Coupled Patch Antenna Using Hybrid 3D / Inkjet Additive Manufacturing Technique," Accepted for presentation at *European Microwave Conf.*, Sept. 2015, Paris, France.

[11] R. Bahr, M. Tentzeris, "RF Characterization of 3D Printed Flexible Materials-NinjaFlex Filaments," Accepted for presentation at *European Microwave Conf.*, Sept. 2015, Paris, France.

[12] Y. Chang, H. Chung, "In Situ Stress and Reliability Monitoring on Plastic Packaging Through Piezoresistive Stress Sensor," *IEEE Trans. components, Packag. and Manufacturing Technology*, vol. 3, Aug. 2013.

[13] T. Yamada et al., "A stretchable carbon nanotube strain sensor for human-motion detection," *Nature Nanotechnology*, vol. 6, Mar. 2011.

[14] R. K. Kramer et al., "Wearable tactile keypad with stretchable artificial skin," in *Proceedings IEEE International Conf. Robotics & Automation*, Cambridge, MA, May 2011, pp. 1103–1107.

[15] J. Rogers, Y. Huang, "A curvy, stretchy future for electronics," in *Proceedings of The National Academy of Sciences of the USA*, , vol. 106 no. 27, June 2009, pp. 10875-10876.

[16] Kevin Bullis, "Additive manufacturing is reshaping aviation," in Material News, Feb 2015 [Online] Available: http://www.technologyreview.com/news/534726/additivemanufacturing-is-reshaping-aviation/.

[17] "Additive manufacturing," in The Economist, May 2014, [Online] Available: http://www.economist.com/news/business/21601528-three dimensional-printing-may-help-entrench-worlds-engineering-giantsheavy-metal.

[18] "Comparable U.S. technology,'' [Online] Available: http://www.wtec.org/loyola/satcom/c2_s1b.htm.

[19] C. Hertleer, A. Tronquo, H. Rogier, L. Vallozzi, "Aperture-coupled patch antenna for integration into wearable textile systems," in IEEE Antennas and Wireless Propagtion Letters, Vol. 6, pp.392-395, August 2007.

[20] D. Pozar, D. Schaubert, "A review of some microstrip antenna characteristics," in Microstrip Antennas, IEEE Press.

[21] J. Kimionis, A. Georgiadis, M. Isakov, H.J. Qi, and M.M. Tentzeris, "3D/Inkjet-printed origami antennas for multi-direction RF Harvesting,"

accepted for presentation to the IEEE MTT-S International Microwave Symposium (IMS) 2015, May 2015, Phoenix, AZ, USA.

[22] D. Pozar, S. Duffy, “A dual-band circularly polarized aperture-coupled stacked microstrip antenna for global positioning satellite,” in IEEE Transactions on Antennas and Propagation, Vol. 45, No. 11, pp.16181625, November 1997.

[23] P. Sullivan, D. Schaubert, “Analysis of an aperture coupled microstrip antenna,” in IEEE Transactions on Aantennas and Propagation, Vol. 34, No. 8, pp.977-984, August 1986.

[24] S. Walker and J. A. Lewis, “Reactive Silver Inks for Patterning HighConductivity Features at Mild Temperatures,” Journal of the American Chemical Society, Vol. 134, No. 3, pp.1419−1421, January 2012.

[25] R. Coccioli, F. Yang, K. Ma, “Aperture-Coupled Patch Antenna on UCPBG Substrate,” in IEEE Transactions on Microwave Theory and Techniques, Vol. 47, No. 11, pp.2123-2130, Nov 1999.

[26] C. Balanis, “Loop Antennas,” in *Antennna theory: analysis and design,* 3rd ed., A John Wiley & Sons, Inc., pp. 256-265.

[27] E. Palermo. (2013, Sept. 19). *Fused Deposition Modeling: Most Common 3D Printing Method* [Online]. Available FTP: http://www.livescience.com/39810-fused-deposition-modeling.html

[28] *Flex Your 3D Imagination* [Online]. Available FTP: http://www.ninjaflex3d.com/about/

[29] L. Golestanirad et al, “Effect of realistic modeling of deep brain stimulation on the prediction of volume of activated tissue,” *Progress In Electromagnetics Research,* vol. 126, 1–16, 2012.

[30] M. T. Islam et al, “Analysis of materials effects on radio frequency electromagnetic fields in human head,” *Progress In Electromagnetics Research,* vol. 128, 121–136, 2012.

[31] [Online] Available FTP: http://proto3000.com/polyjet-matrix-3d-printing-services-process.php

[32] [Online] Available FTP: http://phys.org/news/2015-05-inkjet-kesterite-solar-cells.html

[33] *Specific Absorption Rate (SAR) for Cellular Telephones* [Online]. Available FTP: https://www.fcc.gov/encyclopedia/specific-absorption-rate-sar-cellular-telephones

[34] What is SAR and what is all the fuss about? [Online]. Available FTP: http://sarvalues.com/what-is-sar-and-what-is-all-the-fuss-about/

[35] "Additive manufacturing," in The Economist, May 2014, [Online] Available: http://www.economist.com/news/business/21601528-three-dimensional-printing-may-help-entrench-worlds-engineering-giants-heavy-metal.

[36] "Comparable U.S. technology,'' [Online] Available: http://www.wtec.org/loyola/satcom/c2_s1b.htm.

[37] C. Hertleer, A. Tronquo, H. Rogier, L. Vallozzi, "Aperture-coupled patch antenna for integration into wearable textile systems," in IEEE Antennas and Wireless Propagtion Letters, Vol. 6, pp.392-395, August 2007.

[38] D. Pozar, D. Schaubert, "A review of some microstrip antenna characteristics," in Microstrip Antennas, IEEE Press.

[39] J. Kimionis, A. Georgiadis, M. Isakov, H.J. Qi, and M.M. Tentzeris, "3D/Inkjet-printed origami antennas for multi-direction RF Harvesting," accepted for presentation to the IEEE MTT-S International Microwave Symposium (IMS) 2015, May 2015, Phoenix, AZ, USA.

[40] D. Pozar, S. Duffy, "A dual-band circularly polarized aperture-coupled stacked microstrip antenna for global positioning satellite," in IEEE Transactions on Antennas and Propagation, Vol. 45, No. 11, pp.1618-1625, November 1997.

[41] P. Sullivan, D. Schaubert, "Analysis of an aperture coupled microstrip antenna," in IEEE Transactions on Aantennas and Propagation, Vol. 34, No. 8, pp.977-984, August 1986.